Bayesian Updating with Adaptive, Uncertainty-Informed Subset Simulations: High-fidelity Updating with Multiple Observations

Zeyu Wang[1,2] and Abdollah Shafieezadeh[2]

[1] School of Engineering and Technology, China University of Geosciences (Beijing), Beijing 100083, China

[2] Risk Assessment and Management of Structural and Infrastructure Systems (RAMSIS) lab, Department of Civil, Environmental, and Geodetic Engineering, The Ohio State University, Columbus, OH, USA 43210

ABSTRACT

The well-known *BUS* algorithm (i.e., Bayesian Updating with Structural reliability) transforms Bayesian updating problems into structural reliability to address challenges of updating with equality information and improve computational efficiency. However, as the number of observations increases, the resulting failure probability or acceptance ratio becomes exceedingly small, requiring a formidable number of evaluations of the likelihood function. To overcome this limitation especially for complex computational models, this paper presents a new approach where the probability estimation problem of the very rare event associated with updating is decomposed into a set of sub-reliability problems with uncertain failure thresholds. Two concepts of Conditional Acceptance Rate Curve (CARC) and Dynamic Learning Function (DLF) are proposed to enable precise identification of the intermediate failure thresholds and to train Kriging surrogate models for the established limit state functions. Two benchmark numerical examples and a practical corrosion problem in marine environments are investigated to analyze the efficiency of the proposed method relative to *BUS* and other state-of-the-art methods. Results indicate that the proposed method can reduce computational costs by about an order of magnitude while maintaining high accuracy; therefore, enabling Bayesian updating of complex computational models.

Key words: *Bayesian updating; Bayesian Inference; Calibration; Reliability Analysis; Kriging; Markov Chain Monte Carlo; Subset simulation;*

1. Introduction

Uncertainties in physical phenomena and in models that attempt to represent these phenomena may significantly affect perceptions and subsequently decisions [1]. Although information in many cases may not be directly available for a parameter or response of interest, available observations can be used for indirect inference. These observations such as system capacities, structural deformations, system dynamic features and geometric and material deteriorations can be obtained by the state-of-the-art sensing and monitoring techniques. Therefore, it is highly necessary to derive computational methods to better characterize aforementioned uncertainties and infer probabilistic information for target uncertain responses of interest. As for the mainstream technique of uncertainty quantification, Bayesian updating has the capability to achieve this goal [2].

Bayesian updating while present a solid analytical framework, is computationally very demanding especially when the information is of equality type. This paper aims to substantially improve the computational efficiency of Bayesian updating through deep integration of advanced sampling methods and surrogate modeling. Generally, methodologies for estimating posterior distribution can be categorized into approximation-based approaches such as Laplace approximation [3] and simulation-based techniques such as Markov Chain Monte Carlo sampling (MCMC) [4]. The first category can be computationally efficient for cases with low dimensions, however, their performance degrades as the number of uncertain variables and the complexity of the posterior density increase [5]. On the other hand, samples with posterior distribution can be asymptotically generated through MCMC sampling [1]. The MCMC sampling method relies on the proposal or the so-called jumping function. This process requires the samples following the posterior distribution to be generated in a sequential manner. The previously generated samples affect the proposal sampling function (i.e., uniform distribution or normal distribution) by changing its mean value before each new point is added. However, MCMC sampling may face difficulty in converging to a stationary state if the definition of acceptance rate or the batch size is inappropriate [5]–[7]. To overcome the aforementioned shortcomings, Ching et al. [8], proposed the transitional Markov chain Monte Carlo sampling method (TMCMC) which adaptively generates samples with a group of intermediate probability distributions and asymptotically obtains samples that follow the posterior probability distribution. However, the computational efficiency of the TMCMC sampling method decays as the dimension of the problem increases [5], [9]. By reinterpreting Bayesian updating as a structural reliability problem, Straub and Papaioannou [6] proposed Bayesian Updating with Structural reliability (*BUS*) method. This framework introduces a limit state function through which the accepted samples are equivalently defined as the failure samples in structural reliability problems. It is shown that subset simulation can be leveraged to efficiently generate accepted samples in the process of implementing MCS-based simple rejection sampling algorithm based on the reformulated limit state function [6], [10]–[13]. The subset simulation-based *BUS* method adaptively detects and identifies the path to the acceptance area defined by the equivalent limit state function. Bayesian updating has also been applied to the fields of analysis of rare events, analysis of deteriorating systems, parameter estimation of spatially-varying phenomena, detection-related problems in water distribution networks, remaining useful life estimation and system degradation [14]–[23]. Moreover, Wang and Shafieezadeh [24] proposed *BUAK* to transform the Bayesian updating problem into a system reliability problem and enhance the computational performance of *BUS* with adaptive Kriging-based MCS. Subsequently, Liu and et al. [25], further improved this framework by proposing a variant called *BUS-AK*^{2} to address the case that the magnitude adjusting constant is not known in advance. Moreover, *BUS* has been integrated with adaptive importance sampling [26], [27] for improved performance.

Although *BUS* avoids problems associated with the instability of Markov chain in MCMC sampling by reinterpreting Bayesian updating as a reliability analysis problem, it has a large computational cost which stems from the simulation-based evaluation of the likelihood function. The computational demand increases significantly as the acceptance rate becomes very small [5], [7]. Taking the subset simulation-based *BUS* for example, the total number of evaluations of the likelihood function N_{call} can be determined as [6],

$$N_{call} = N_{ss} \cdot N_{in} + N_t - N_{ts} \tag{1}$$

where N_{ss} denotes the number of subsets, N_{in} is the number of samples in each intermediate subset, N_t is the number of target samples and N_{ts} is the number of seeds in the final subset. Though N_{call} estimated through subset simulation is relatively smaller compared to the crude Monte Carlo simulation or MCMC, it can easily reach thousands or even larger for sophisticated models. An efficient way to significantly reduce N_{call} is to use surrogate models. It is known that many state-of-the-art surrogate models or machine learning tools [28] such as Response Surface [7], [8], [9], Polynomial Chaos Expansion [32], Support Vector Regression [33], [34], Physics-informed Neural Networks (PINN) [35] or Kriging [36], [37] have great computational efficiency in solving structural reliability problems. As one of the most promising techniques, Kriging-based reliability analysis methods have achieved high accuracy and computational efficiency [13], [36], [38], [39], [40]. However, the very small acceptance rate caused by the large number of observations makes the direct implementation of regular Kriging-based reliability analysis methods very inefficient. This limitation stems from the fact that a significantly large number of candidate design samples should be prepared to realize the failure or accepted areas, otherwise the Kriging surrogate model cannot guarantee the accuracy for the point classification task of MCS [36]. Therefore, we propose *BUS-SSAK* to control the number of candidate design samples, substantially reduce the computational cost while achieving a robust and high accuracy.

Building on the *BUS* approach, *BUS-SSAK* adaptively searches for seeds that are located in the accepted domain via the construction of Kriging surrogate models and subsequently generates samples through MCMC technique based on the well-constructed Kriging models. However, a critical challenge for this integration is finding intermediate acceptance thresholds. Two models called CARC and DLF are proposed to identify the thresholds in the acceptance regions, while facilitating adaptive training of the Kriging models. CARC is a novel model that builds a relation between the changeable intermediate failure threshold and intermediate failure probability. On the other hand, DLF is a novel learning function that can strategically add training samples according to the changeable intermediate failure threshold. Using the analytical derivation of the confidence intervals for the intermediate failure probability, the intermediate failure thresholds are adaptively identified as more training samples are added in the Kriging surrogate model. These new capabilities in *BUS-SSAK* facilitate accurate estimation of posterior distributions with high computational efficiency without the need to investigate a large number of evaluations to the likelihood function for all candidate design samples in each subset. This consequently enables Bayesian updating of computationally complex models, where each run of the model can be very costly. One should note that the work represented in [24] is the first attempt in incorporating the *BUS* algorithm with *AK-MCS* to improve the performance of Bayesian updating. It is found that *BUAK* becomes increasingly inefficient and Kriging experiences substantial computational burden when the acceptance rate decreases, or the number of observations increases. Inspired by the fact that subset simulation can successfully tackle reliability problems with small failure probability, this paper proposes integrating Kriging with subset simulation to address these limitations. CARV and DLF are two proposed concepts that are devised to facilitate this integration. Therefore, the major novel contribution of this research lies in the proposed *BUS-SSAK* algorithm that enables Bayesian updating with small acceptance rate and control the computational demand, which is significantly different from the classic Bayesian Updating method such as ABC-SubSim [42].

In the remaining parts of this paper, the elements of *BUS* method and subset simulation are briefly introduced in Section 2. In Section 3, the proposed method that integrates the state-of-the-art *BUS* method and Kriging-based subset simulation technique (i.e., methods for seeking the seeds and generating samples with posterior distribution) is elaborated. To investigate the computational performance of *BUS-SSAK*, four numerical examples are implemented in Section 4. In Section 5, the conclusions of this research are presented.

2. Background

While physical models become increasingly sophisticated in a deterministic sense, input and model uncertainties still persist and must be dealt with. Characterizing and reducing these uncertainties are critical for the understanding of the phenomena and decisions that may rely on these models. In many cases, however, it is not affordable either technologically or cost-wise to collect information directly for the uncertainties of interest. For example, for constructed structures that are in service determining the stiffness of its structural components via destructive testing is impractical. The uncertainty of the structural stiffness, however, can be deduced via statistical inference using other auxiliary observations such as eigen frequencies of the structure [6]. Bayesian updating, regarded as an efficient tool for uncertainty quantification, assumes an empirical prior probability distribution for unknown parameters (i.e., the structural stiffness in the previous example). Let $f(\boldsymbol{x})$ denote the probability density function(pdf) of assumed prior distribution of unknown variables and $f'(\boldsymbol{x})$ represents the pdf of posterior distribution of $\boldsymbol{x}$. Therefore, the Bayesian updating formulation can be represented as follows,

$$f'(\boldsymbol{x}) = \frac{L(\boldsymbol{x})f(\boldsymbol{x})}{\int_{\boldsymbol{X}} L(\boldsymbol{x})f(\boldsymbol{x})d\boldsymbol{x}} \tag{2}$$

where $\boldsymbol{X}$ is the random variable, $\boldsymbol{x}$ is a stochastic realization of $\boldsymbol{X}$ and $L(\boldsymbol{x})$ is the likelihood function, which is proportional to the conditional probability of observations according to [6],

$$L(\boldsymbol{x}) \propto \Pr(Z|\boldsymbol{X} = \boldsymbol{x}) \tag{3}$$

where Z denotes the concept of event. If the MCMC technique is adopted to estimate $f'(\boldsymbol{x})$, the denominator in Eq. (2) is trivial as numerator can be easily normalized to one [5]. Typically, the likelihood function $L(\boldsymbol{x})$ is composed of three parts: observations Z, responses from the model $h(\boldsymbol{x})$ and error ε, which reflects the difference between $h(\boldsymbol{x})$ and Z. Concerning the measuring error and modeling errors, the corresponding relation can be represented as,

$$\varepsilon = Z - h(\boldsymbol{x}) \tag{4}$$

In Eq. (4), it is assumed that the information and errors can be directly observed and measured in the majority of engineering cases. However, there are situations where likelihood function is not linear around the error term [41]. For cases where linear representation is adequate, if the probability density function (PDF) of the error ε is known, $L(\boldsymbol{x})$ can be parameterized by the observation and the responses from the model as,

$$L(\boldsymbol{x}) = \varphi_{\varepsilon}(\varepsilon) = \varphi_{\varepsilon}(Z - h(\boldsymbol{x})) \tag{5}$$

where $\varphi_{\varepsilon}(\cdot)$ denotes the PDF of ε. Note that the likelihood function in Eq. (5) can be decomposed into m sub-likelihood functions $L_i(\boldsymbol{x}), \mathrm{i} = 1,2, \dots, m_l$, which can be represented as,

$$L(\boldsymbol{x}) = \prod_{i=1}^{m_l} L_i(\boldsymbol{x}) = \prod_{i=1}^{m_l} \varphi_{\varepsilon}(Z_i - h_i(\boldsymbol{x})) \tag{6}$$

where m_l denotes the number of mutually independent measurements. In this article, it is assumed that the likelihood functions are mutually independent.

2.1. Bayesian Updating with Structural Reliability Methods

As stated in Introduction, the stability of the Markov chain through conventional MCMC algorithms may not be guaranteed if the sample size is insufficient. To address this limitation, Straub and Papaioannou [6] proposed *BUS* (Bayesian Updating with Structural reliability methods) to take advantage of structural reliability methods to improve the accuracy and efficiency of estimating $f'(\boldsymbol{x})$. *BUS* implements Simple Rejection Method (*SRM*), which is briefly reviewed in this subsection. Note that the accepted domain Ω_{acc} can be defined based on the augmented outcome space $[\boldsymbol{x}, p]$ where *P* is an auxiliary uniform random variable with its random realizations represented by p,

$$\Omega_{acc} = [p \leq cL(\boldsymbol{x})] = [h(\boldsymbol{x}, p) \leq 0] \tag{7}$$

where,

$$h(\boldsymbol{x}, p) = p - cL(\boldsymbol{x}) \tag{8}$$

$h(\boldsymbol{x}, p)$ is the equivalent limit state function parameterized by the random variables $[\boldsymbol{x}, p]$ and c is a constant satisfying $cL(\boldsymbol{x}) \leq 1$ for all the outcomes of $\boldsymbol{X}$. c can be defined as,

$$c = \frac{1}{max(L(\boldsymbol{x}))} \tag{9}$$

The posterior distribution $f'(\boldsymbol{x})$ can be defined as,

$$f'(\boldsymbol{x}) = \frac{\int_{p \in \Omega_{acc}} f(\boldsymbol{x}) dp}{\int_{[x,p] \in \Omega_{acc}} f(\boldsymbol{x}) dp d\boldsymbol{x}} = \frac{\int_0^1 I^{acc}([\boldsymbol{x}, p] \in \Omega_{acc}) f(\boldsymbol{x}) dp}{\int_{\boldsymbol{X}} \int_0^1 I^{acc}([\boldsymbol{x}, p] \in \Omega_{acc}) f(\boldsymbol{x}) dp d\boldsymbol{x}} \tag{10}$$

where $I^{acc}([\boldsymbol{x}, p] \in \Omega_{acc})$ is the indicator function corresponding to the structural reliability problem with limit state function $h(\boldsymbol{x}, p) = p - cL(\boldsymbol{x})$. The corresponding numerator and denominator in Eq. (10) can be further expanded as,

$$\int_{p\in\Omega_{acc}} f(\boldsymbol{x})dp = \int_0^{cL(\boldsymbol{x})} f(\boldsymbol{x})dp = cL(\boldsymbol{x})f(\boldsymbol{x}) \tag{11}$$

and

$$\int_{[x,p]\in\Omega_{acc}} f(\boldsymbol{x})dpd\boldsymbol{x} = \int_{\boldsymbol{X}}\int_0^1 I^{acc}([\boldsymbol{x},p]\in\Omega_{acc})f(\boldsymbol{x})dpd\boldsymbol{x} = \int_{\boldsymbol{X}}\left\{\int_0^1 I^{acc}\big(p\le cL(\boldsymbol{x})\big)dp\right\}f(\boldsymbol{x})d\boldsymbol{x} = \int_{\boldsymbol{X}} cL(\boldsymbol{x})f(\boldsymbol{x})d\boldsymbol{x} \tag{12}$$

Eq. (11) and (12) are the exact formulations in Eq. (10). In this context, the simple rejection sampling algorithm is summarized and presented in Algorithm 1. The simple rejection sampling algorithm faces the limitation that the acceptance rate is low. This rate significantly decreases as the number of observations m increases. Straub and Papaioannou [6] pointed out that the average acceptance rate is proportional to $\frac{1}{\sqrt{m}}$, when all measurements are independent and identically distributed (iid). This limitation makes the process of Bayesian updating computationally intractable since only very few accepted samples can be used to estimate the posterior distribution, while a large number of unnecessary samples are prepared. This limitation becomes a major challenge for sophisticated, time-consuming models such as high-fidelity Finite Element models.

Algorithm 1. Simple Rejection Sampling

1. $i = 1$
2. Generate a sample $\boldsymbol{x}^i$ from $f(\boldsymbol{x})$
3. Generate a sample p^i from the standard uniform distribution $[0,1]$
4. If $[\boldsymbol{x}^i, p^i] \in \Omega_{acc}$
   (a) Yes, accept $\boldsymbol{x}^i$, $i = i + 1$
   (b) No, reject $\boldsymbol{x}^i$, $i = i$
5. Stop if $i = N_s$, else go to step 2

2.2. BUS with Subset Simulation (SS)

In this subsection, the subset simulation method for estimating the probability of failure is first reviewed. Subsequently, the integration of *BUS* with Subset simulation algorithm is explained. Different from the goal in Bayesian updating, structural reliability methods are aimed at estimating the probability of failure as follows,

$$P_f = P(h(\boldsymbol{X}) \le 0) \tag{13}$$

where P_f denotes the probability of failure and $h(\boldsymbol{X})$ is the so-called limit state function or performance function in structural reliability problems: $h(\boldsymbol{X}) \le 0$ indicates failure and $h(\boldsymbol{X}) > 0$ means safe state. The contour where $h(\boldsymbol{X}) = 0$ is called the limit state. Au and Beck [10] proposed subset simulation to estimate the probability of failure, here denoted as $\hat{P}_f^{ss}$, by decomposing of the original limit state function into a series of easily computable LSFs with intermediate failure thresholds. Generally, let the subsets be divided as $\Omega_1 \supset \Omega_2 \supset \cdots \supset \Omega_m = \Omega_f$ and $\Omega_f = \bigcap_{i=1}^{m}\Omega_i$, where Ω_f denotes the failure domain. Therefore, the subsets Ω_is are the failure domains that correspond to the LSFs as follows,

$$\Omega_i = \{\boldsymbol{x}: h(\boldsymbol{x}) \le t_i\} \tag{14}$$

where t_is are the intermediate failure thresholds that satisfy $t_1 > t_2 > \cdots > t_m = 0$. The process of subset simulation is illustrated in Fig. 1. The failure probability using subset simulation $\hat{P}_f^{ss}$ can be estimated as,

$$P_f \approx \hat{P}_f^{ss} = \mathrm{P}(\Omega_m) = \mathrm{P}\left(\bigcap_{i=1}^{m} \Omega_i\right) = \mathrm{P}(\Omega_1) \cdot \prod_{i=1}^{m-1} \mathrm{P}(\Omega_{i+1}|\Omega_i) \quad (15)$$

where $\mathrm{P}(\Omega_1)$ and $\mathrm{P}(\Omega_{i+1}|\Omega_i)$ are determined through crude Monte Carlo simulation with the following intermediate limit state functions $h(\boldsymbol{x}) \leq t_i$. The intermediate conditional probability can be commonly set as: $\mathrm{P}(\Omega_{i+1}|\Omega_i) \approx p_0 = 0.1$. However, p_0 is not merely a fixed value and can be set toward an optimal goal. Interested readers can refer to [42] for more information. Finally, the probability of failure through subset simulation is estimated as,

$$\hat{P}_f^{ss} = \mathrm{P}(\Omega_1) \cdot \prod_{i=1}^{m-1} \mathrm{P}(\Omega_{i+1}|\Omega_i) = P_0^{m-1} \hat{P}_0^{m} \quad (16)$$

Details of the implementation for subset simulation is summarized in Algorithm 1A of Appendix 1.

Note that subset simulation technique is aimed at estimating the probability of failure $\hat{P}_f^{ss}$, which is different from the goal of *BUS* that is drawing all the failure (acceptable) samples. By adjusting the procedure in subset simulation for estimating the probability of failure, *BUS* focuses on the strategy to draw failure samples. The modified methodology that integrates *BUS* and subset simulation is summarized in Algorithm 1B of Appendix 1. However, even with integrated with subset simulation, *BUS* faces several challenges. First, the acceptance rate becomes significantly small as the number of observations increases. In this circumstance, estimating posterior distributions using *BUS* become equivalent to analyzing the reliability of rare events, which becomes rather computationally expensive for simulation-based approaches including subset simulation. As shown in Eq. (1), N_{call} can easily reach thousands in *BUS* with subset simulation. Although this number is relatively smaller compared to the crude Monte Carlo simulation or MCMC, it is still computationally inefficient for Bayesian updating when sophisticated computational models are involved. Kriging-based reliability analysis methods are known for their capabilities in substituting time-consuming performance functions and improving the computational efficiency [36]. Note that, there are two crucial steps in the implementation of *BUS* and subset simulation: identifying the seeds located in or close to the failure domain and drawing the samples following $f'(\boldsymbol{x})$ in the final failure subset (acceptance domain). The first step is computationally demanding since it requires a large number of evaluations to explore the path to failure domain. The goal of this paper is to efficiently search for the seeds or the path to the failure domain with the assistance of Kriging surrogate models. This approach can substantially reduce the computational demand associated with large samples drawn in each intermediate subset. Moreover, Kriging-based reliability analysis is also adopted in the final subset to draw the target failure samples. Details of this approach are elaborated in the next section.

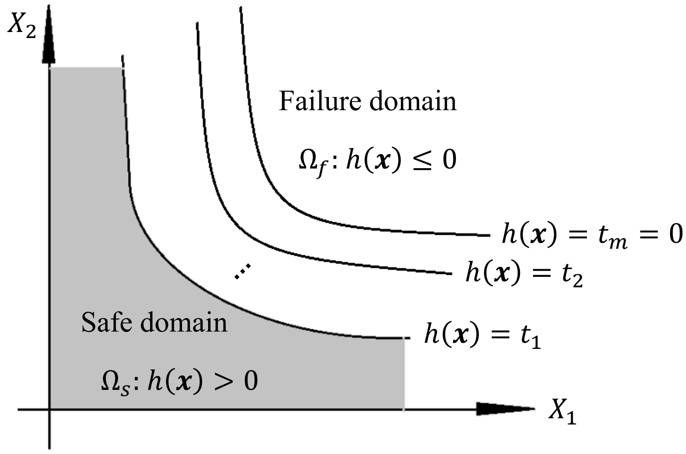

Fig. 1. 2D illustration of subset simulation.

3. Bayesian Updating with Subset Simulation using Adaptive Kriging

This section presents a new approach to Bayesian updating via integration of *BUS* and Kriging-based subset simulation. This method, called *BUS-SSAK*, substantially improves the computational efficiency of Bayesian updating. The elements of Kriging model are briefly recapped in Appendix 2. Generally, this paper aims to significantly improve the performance of *BUS-SS* algorithm by strategically incorporating adaptive Kriging surrogate models. However, when a surrogate model is introduced, reaching the set thresholds cannot be guaranteed; therefore, finding the intermediate acceptance threshold in this integration process becomes very critical, as it is detrimental to the outcome of reliability analysis. Toward this goal, we proposed two techniques called Conditional Acceptance Rate Curve (CARC) and Dynamic Learning Function (DLF) to identify the intermediate failure thresholds in the acceptance regions. CARC establishes a relation between the intermediate failure threshold and intermediate failure probability and estimates the corresponding confidence intervals. DLF supports identifying optimal training samples for the Kriging surrogate model. The process of *BUS-SSAK* can be briefly explained as follows. Initially, a number of candidate design samples are generated via the crude MCS technique and the training samples are randomly selected from these candidate design samples. Subsequently, the Kriging model is constructed based on the selected training samples. As training proceeds, the ratio of the width of the confidence intervals of estimated failure probability to the estimated failure probability in the vicinity of the estimated intermediate failure threshold reduces, which facilitates gradual identification of the intermediate failure threshold. After an intermediate failure threshold is accurately identified, the seeds for implementing MCMC in the next subset are prepared. The seeds searching process is repeated several times (i.e., the same process followed in regular subset simulation) until the identified intermediate threshold is smaller than zero. Eventually, the seeds for generating samples with the posterior distribution via MCMC can be obtained in the accepted domain. By implementing adaptive Kriging-based reliability method based on candidate design samples in the last subset, the Kriging surrogate model can be well constructed. Samples with posterior distribution can be finally generated based on the well-trained Kriging surrogate model and the seeds identified in the last subset. By adaptively identifying the acceptable samples and searching for the path to the failure domain, *BUS-SSAK* can significantly reduce the number of evaluations to the likelihood function and simultaneously maintain a desirable accuracy. Details of this method is elaborated in the following subsections.

3.1. Seed Seeking using Adaptive Kriging

It is known that subset simulation is aimed adaptively identifying the intermediate thresholds $t_i, i = 1, 2, \ldots, m$ until t_m is smaller than zero,

$$P(\Omega_{i+1}|\Omega_i) = P(h(\boldsymbol{x}) \leq t_i) = p_0\,, \qquad \boldsymbol{x} \in \Omega_i \tag{17}$$
$$s.t.\, t_i \geq 0$$

where $g(\boldsymbol{x})$ is the limit state function in structural reliability problems and p_0 is the conditional failure probability in each subset. Eq. (17) is normally interpreted in the context of reliability analysis. Here, we redefine p_0 as the conditional acceptance rate in *BUS* + *SS*. Note that the true performance function $h(\boldsymbol{x})$ should be substituted by the Kriging surrogate model $\hat{h}(\boldsymbol{x})$, which means the true value of t_i in Eq. (17) cannot be precisely identified. Therefore, the key point of *BUS*+*SSAK* is to identify a value $\hat{t}_i$ so that $\hat{t}_i \cong t_i$ as the training samples enrich the Kriging surrogate model. To enable accurate identification of t_i, two new concepts are introduced. First, we introduce Conditional Acceptance Rate Curve (CARC) that represents the relation between the conditional failure probability and the conditional acceptance ratio (i.e., equivalent to the conditional failure probability in reliability estimation),

$$\hat{P}_{acc}^{c}(t^*) = P\big(\hat{h}(\boldsymbol{x}) \leq t^*\big), \qquad t^* \geq 0 \tag{18}$$

where t^* is a variable that needs to be adaptively estimated and $\hat{P}_{acc}^{c}(t^*)$ represents the conditional failure probability parameterized by variable t^*. In this article, the probabilistic classification-based Monte Carlo simulation (PC-MCS) is adopted to estimate $\hat{P}_{acc}^{c}(t^*)$ as follows,

$$\hat{P}_{acc}^{c}(t^*) = \frac{1}{N_{in}}\sum_{i=1}^{N_{in}} I_{\hat{h}}(\boldsymbol{x}_i, t^*) = \frac{1}{N_{in}}\sum_{i=1}^{N_{in}} \Phi\left(\frac{-(\mu_{\hat{h}}(\boldsymbol{x}_i) - t^*)}{\sigma_{\hat{h}}(\boldsymbol{x}_i)}\right), \tag{19}$$

where N_{in} is the number of samples in each subset, $I_{\hat{h}}(\cdot)$ is a probabilistic indicator that measures the probability of $\boldsymbol{x}_i$ belonging to acceptance domain (i.e., equivalent to failure in reliability estimation) and $\mu_{\hat{h}}(\cdot)$ and $\sigma_{\hat{h}}(\cdot)$ are the mean value and standard deviation estimated from the Kriging model, respectively. Details of this probabilistic classification-based MCS have been documented in the literature [43]–[45]. As shown in Fig 2. (a), the confidence intervals can be estimated with Kriging model trained by several samples $\boldsymbol{x}_{tr}$. Note that if $\hat{t}$ changes, the failure probability estimated through the PC-MCS also changes. In Fig. 2, the black solid and red dashed lines denote the mean and confidence interval (CI) of $\hat{P}_{acc}^{c}$, respectively. Moreover, $\hat{t}$ is the estimated intermediate failure threshold with maximum likelihood satisfying Eq. (17), which subsequently leads to,

$$P\big(\hat{h}(\boldsymbol{x}) \leq \hat{t}\big) = p_0\,, \qquad \boldsymbol{x} \in \Omega_i, \qquad i = 1,2,\dots,m \tag{20}$$

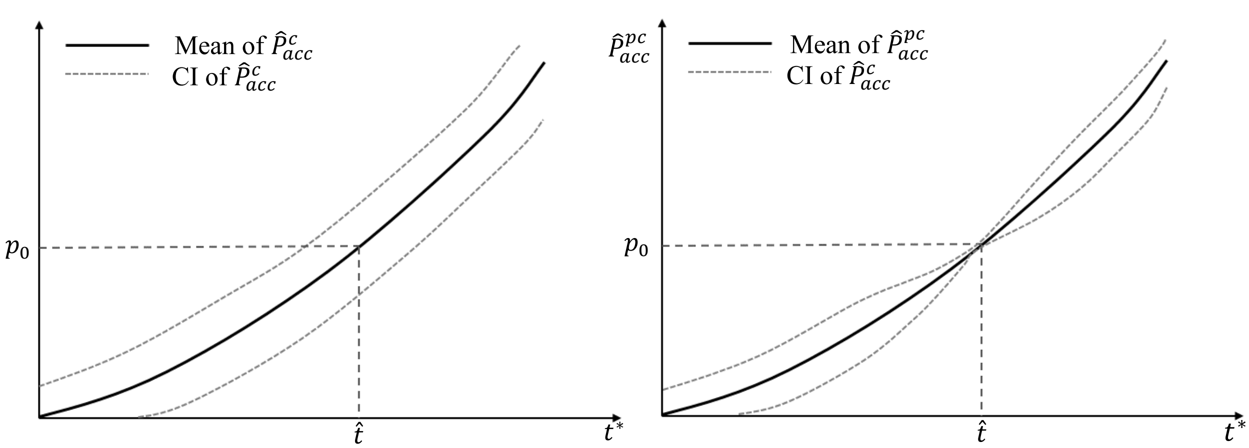

(a) (b)

Fig. 2. Conditional Acceptance Rate Curve (CARC) with (a) merely initial training samples and (b) sufficient training samples in the vicinity of the limit state $\hat{h}(\boldsymbol{x}) - \hat{t} = 0$.

As the training samples in the Kriging surrogate model increases, $\hat{t} = t_i$ is asymptotically satisfied. The CI for $\hat{P}_{acc}^{c}$ can be obtained using the approach proposed by the authors in [43]. If the current subset of candidate design samples is denoted as Ω_i, then the conditional acceptance rate can be computed as,

$$\hat{P}_{acc}^{c}(t^*) = \frac{\hat{N}_{acc}^{c}(t^*)}{N_{in}} \tag{21}$$

where $\hat{N}_{acc}^{c}$ is the expected number of accepted samples in Ω_i. In this approach, for each candidate design sample, $\boldsymbol{x}_i$, the outcome of the indicator function follows a Bernoulli distribution,

$$I_{\hat{h}}(\boldsymbol{x}, t^*) \sim B\left(\mu_b(\boldsymbol{x}, t^*), \sigma_b^2(\boldsymbol{x}, t^*)\right), \boldsymbol{x} \in \Omega_i, i = 1,2, \dots, m \tag{22}$$

where B denotes the Bernoulli distribution, $\mu_b(\boldsymbol{x}_i)$ is the Bernoulli mean with $\mu_{\mathrm{b}}(\boldsymbol{x}, t^*) = \Phi\left(\frac{-(\mu_{\hat{h}}(\boldsymbol{x}) - t^*)}{\sigma_{\hat{h}}(\boldsymbol{x})}\right)$ and σ_b^2 is the corresponding variance with $\sigma_b^2(\boldsymbol{x}, t^*) = \mu_{\mathrm{b}}(\boldsymbol{x}, t^*)\left(1 - \mu_{\mathrm{b}}(\boldsymbol{x}, t^*)\right)$. Since $\hat{N}_{acc}^{c}$ can be regarded as the expected value of the sum of $I_{\hat{h}}(\boldsymbol{x}, t^*)$, $\boldsymbol{x} \in \Omega_i$, it follows a Poisson binomial distribution (PBD). According to [43], the distribution of $\hat{N}_{acc}^{c}(t^*)$ can be denoted as,

$$\hat{N}_{acc}^{c}(t^*) \sim PB\left(\mu_{\hat{N}_{acc}^{c}}(t^*), \sigma_{\hat{N}_{acc}^{c}}^2(t^*)\right) \tag{23}$$

where $\mu_{\hat{N}_{acc}^{c}}(t^*)$ and $\sigma_{\hat{N}_{acc}^{c}}^2(t^*)$ are the mean value and variance of $\hat{N}_{acc}^{c}(t^*)$, respectively. It can be shown that $\mu_{\hat{N}_{acc}^{c}}(t^*) = \sum_{i=1}^{N_{in}} \mu_{\mathrm{b}}(\boldsymbol{x}, t^*)$ and $\sigma_{\hat{N}_{acc}^{c}}^2(t^*) = \sum_{i=1}^{N_{in}} \mu_{\mathrm{b}}(\boldsymbol{x}, t^*)\left(1 - \mu_{\mathrm{b}}(\boldsymbol{x}, t^*)\right)$. Therefore, the CI of $\mu_{\hat{N}_{acc}^{c}}(t^*)$ can be determined as,

$$\hat{N}_{acc}^{c}(t^*) \in \left(\boldsymbol{\Theta}_{\hat{N}_{acc}^{c}}^{-1}\left(\frac{\alpha}{2}, t^*\right), \boldsymbol{\Theta}_{\hat{N}_{acc}^{c}}^{-1}\left(1 - \frac{\alpha}{2}, t^*\right)\right) \tag{24}$$

where $\boldsymbol{\Theta}_{\hat{N}_{acc}^{c}}^{-1}(\cdot)$ is the inverse cumulative distribution function of PBD with mean $\mu_{\hat{N}_{acc}^{c}}(t^*)$ and variance $\sigma_{\hat{N}_{acc}^{c}}^2(t^*)$ and α is the confidence level (e.g. $\alpha = 0.05$). For computational simplicity, the Central Limit Theorem shows that $\hat{N}_{acc}^{c}(t^*)$ follows a normal distribution [43],

$$\hat{N}_{acc}^{c}(t^*) \sim N\left(\mu_{\hat{N}_{acc}^{c}}(t^*), \sigma_{\hat{N}_{acc}^{c}}^2(t^*)\right) \tag{25}$$

It should be noted that the approximation of Poisson Binomial distribution to a Normal distribution has been demonstrated in [43]. Moreover, PBD should be treated as a Poisson distribution if N_{in} is set to be as small as $N_{in} \leq 50$. However, for all numerical cases here, $N_{in} \geq 5000$, which is sufficiently large to guarantee that PBD can be well approximated by a Normal distribution according to the CLT. Therefore, the CI of $\hat{N}_{acc}^{c}$ parameterized by the confidence interval α can then be obtained as,

$$\hat{N}_{acc}^{c}(t^*) \in \left[\mu_{\hat{N}_{acc}^{c}}(t^*) - \gamma_{ci}\sigma_{\hat{N}_{acc}^{c}}(t^*),\ \mu_{\hat{N}_{acc}^{c}}(t^*) + \gamma_{ci}\sigma_{\hat{N}_{acc}^{c}}(t^*)\right], \tag{26}$$

where $\gamma_{ci} = 1.96$ for the confidence level $\alpha = 0.05$. As N_{in} is large in Kriging-based reliability analysis problems, the above confidence bounds for $\widehat{N}_{acc}^{c}(t^*)$ are accurate. Accordingly, the CI for $\widehat{P}_{acc}^{c}(t^*)$ can be derived by combining Eq. (21) and (26),

$$\widehat{P}_{acc}^{c}(t^*) \in \frac{1}{N_{in}}\left[\mu_{\widehat{N}_{acc}^{c}}(t^*) - \gamma_{ci}\sigma_{\widehat{N}_{acc}^{c}}(t^*),\ \mu_{\widehat{N}_{acc}^{c}}(t^*) + \gamma_{ci}\sigma_{\widehat{N}_{acc}^{c}}(t^*)\right], \quad \boldsymbol{x} \in \Omega_i, i = 1,2,\dots,m \tag{27}$$

It is clear that the confidence bound of $\widehat{P}_{acc}^{c}$ tightens as training samples in the Kriging model increase and accumulate in the vicinity of the limit state $\hat{h}(\boldsymbol{x}) - \hat{t} = 0$ as shown in Fig. 2. However, lack of strategic selection of training samples from the candidate design samples in each subset can lead to unnecessary training or even incorrect identification of $\hat{t}$. Therefore, it is necessary to develop an approach to strategically select next training samples. In the next section, a new learning function is introduced for optimal selection of training samples so that the uncertainty of $\hat{t}$ or $\widehat{P}_{acc}^{c}$ can be significantly reduced.

3.2. Dynamic Learning Function

In this section, an active learning function is introduced to adaptively refine the Kriging model and asymptotically identify the intermediate acceptance (failure) threshold t_i in Eq. (17). First, let $\boldsymbol{x}_{tr}^*$ denote the selected next best training point that aims to optimally reduce the uncertainty $\sigma_{\widehat{N}_{acc}^{c}}^{2}(\hat{t})$ as follows,

$$\boldsymbol{x}_{tr}^* = \arg\max_{\boldsymbol{x} \in \Omega_i}\left\{\sigma_{\widehat{N}_{acc}^{c}}^{before}(\hat{t}) - \sigma_{\widehat{N}_{acc}^{c}}^{after}(\hat{t})\right\}, i = 1,2,\dots,m \tag{28}$$

where $\sigma_{\widehat{N}_{acc}^{c}}^{before}(\hat{t})$ and $\sigma_{\widehat{N}_{acc}^{c}}^{after}(\hat{t})$ denote the standard deviation, $\sigma_{\widehat{N}_{acc}^{c}}$, of $\widehat{N}_{acc}^{c}$ at $t^* = \hat{t}$ before and after the new training point enriches the Kriging model, respectively. After enrichment by the new training point $\boldsymbol{x}_{tr}^*$, it can be shown that the mean value $\mu_{\mathrm{b}}(\boldsymbol{x}_{tr}^*, \hat{t})$ limits to 0 or 1 and $\sigma_b^2(\boldsymbol{x}_{tr}^*, \hat{t})$ limits to 0,

$$\mu_{\mathrm{b}}(\boldsymbol{x}_{tr}^*, \hat{t}) = \Phi\left(\frac{-(\mu_{\hat{h}}(\boldsymbol{x}_{tr}^*) - \hat{t})}{\sigma_{\hat{h}}(\boldsymbol{x}_{tr}^*) \to 0}\right) = 0 \text{ or } 1, \sigma_b^2(\boldsymbol{x}_{tr}^*, \hat{t}) = \mu_b(\boldsymbol{x}_{tr}^*, \hat{t})\left(1 - \mu_b(\boldsymbol{x}_{tr}^*, \hat{t})\right) = 0 \tag{29}$$

Without considering Kriging correlation, Eq. (28) can be further interpreted by combining Eq. (28) and Eq. (29),

$$\boldsymbol{x}_{tr}^* = \arg\max_{\boldsymbol{x} \in \Omega_i} \sigma_b^2(\boldsymbol{x}, \hat{t}), i = 1,2,\dots,m \tag{30}$$

This equation can be expanded as follows,

$$\boldsymbol{x}_{tr}^* = \arg\max_{\boldsymbol{x} \in \Omega_i}\left[\Phi\left(\frac{-(\mu_{\hat{h}}(\boldsymbol{x}) - \hat{t})}{\sigma_{\hat{h}}(\boldsymbol{x})}\right)\left(1 - \Phi\left(\frac{-(\mu_{\hat{h}}(\boldsymbol{x}) - \hat{t})}{\sigma_{\hat{h}}(\boldsymbol{x})}\right)\right)\right], \quad i = 1,2,\dots,m \tag{31}$$

The procedure to adaptively estimate the true intermediate acceptance ratio t_i is presented in Algorithm 2. The corresponding stopping criterion for dynamic active learning can be set as,

$$\hat{t} \cong t_i \text{ when } \Gamma = \frac{\sigma_{\widehat{N}_{acc}^{c}}}{\mu_{\widehat{N}_{acc}^{c}}} \le \Gamma_{thr} \tag{32}$$

where Γ is the stopping measure and Γ_{thr} is the corresponding stopping threshold. At the beginning of the process, $\hat{t}$ may not be highly accurate to satisfy $\hat{t} = t_i$ as the number of initial training samples is likely insufficient for that purpose. However, $\hat{t}$ asymptotically converges to t_i as new optimal training samples in the vicinity of the limit state $\hat{h}(\boldsymbol{x}) - \hat{t} = 0$ are identified and used in the refinement of the Kriging model. Two dynamic processes constitute the adaptive core of the proposed algorithm. First, the uncertainty or the variance at $\hat{t}$ (e.g. $\sigma_b^2(\boldsymbol{x}, \hat{t})$) is gradually reduced as new training samples are identified and used through the proposed dynamic learning function. Second, $\hat{t}$ is also adaptively estimated as it converges to the true one (e.g., t_i in Eq. (17)) with the addition of the new training samples.

Algorithm 2. Searching for t_i using dynamic learning function and CARC

1. Prepare the initial training samples $\boldsymbol{x}_{in}$ and keep $\boldsymbol{x}_{in}$ and $g(\boldsymbol{x}_{in})$ unchanged for all simulations. Also generate candidate design samples S_i from the subset Ω_i (if $i \geq$ 2)
2. Construct the Kriging model $\hat{h}_i(\cdot)$ based on the current training samples $\boldsymbol{x}_{tr}$
3. Build the Conditional Acceptance Rate Curve (CARC) according to Eq. (19)
4. Search for $\hat{t}$ according to Eq. (20)
5. Search for next training point $\boldsymbol{x}_{tr}^*$ using dynamic learning function according to Eq. (31) and update the training samples $\boldsymbol{x}_{tr}$
6. Check if the stopping criterion is satisfied according to Eq. (32):
   (a) If satisfied, go to step 7.
   (b) If not satisfied, estimate the response for $\boldsymbol{x}_{tr}^*$ and return to step 2.
7. Report $\hat{t}$.

3.3. Estimating Posterior Distributions

Algorithm 2 can determine if the identified intermediate failure threshold t_i in the current subset Ω_i satisfies $\hat{t} \cong t_i > 0$. After $\hat{t} \cong t_i < 0$ and the seeds located in the failure (acceptance) domain are identified and the last Kriging surrogate is well trained $\hat{h}(\boldsymbol{x}) = 0$, samples following the posterior distribution can be drawn in the final step of *BUS+SS*. Subsequently, the problem is slightly changed to the equivalent structural reliability problem as follows,

$$P(\Omega_m | \Omega_{m-1}) = P(h(\boldsymbol{x}) \leq t_m) = P(h(\boldsymbol{x}) \leq 0)\,, \qquad \boldsymbol{x} \in \Omega_{m-1} \tag{33}$$

Similar to the goal of structural reliability analysis that seeks for failure samples, Bayesian updating is aimed at drawing acceptance samples. After the candidate design samples S_{m-1} are drawn from the subset Ω_{m-1}, estimating the posterior distribution can be reinterpreted as a classification problem. Therefore, the estimated limit state with Kriging surrogate model in the last subset (i.e., $\hat{h}(\boldsymbol{x}) = 0$) plays a very important role in this classification task. Algorithm 3 elaborates the process for achieving this goal.

Algorithm 3. Draw acceptance samples in the last subset

1. Generate candidate design samples S_{m-1} from the subset Ω_{m-1}
2. Construct the Kriging model $\hat{h}_m(\cdot)$ based on current training samples $\boldsymbol{x}_{tr}$
3. Estimate the mean $\sigma_{\hat{h}}(\boldsymbol{x})$ and standard deviation $\sigma_{\hat{h}}(\boldsymbol{x})$ for S_{m-1} with $\hat{h}_m(\cdot)$
4. Search for the next best training samples $\boldsymbol{x}_{tr}^*$ using the learning function in Eq. (31), where $\hat{t} = 0$. Update the training samples $\boldsymbol{x}_{tr}$
5. Check if the stopping criterion is satisfied or not:
   (a) If satisfied, go to step 7
   (b) If not satisfied, estimate the response $g(\boldsymbol{x}_{tr}^*)$ for $\boldsymbol{x}_{tr}^*$ and go back to Step 3
6. The limit state $\hat{h}(\boldsymbol{x}) = 0$ is accurately defined

After the estimated limit state $\hat{h}(\boldsymbol{x}) = 0$ is accurately defined, samples following posterior distribution can be drawn according to the last step in *BUS+SS* algorithm but based on the well-trained Kriging surrogate model i.e., $\hat{h}(\boldsymbol{x})$. The last step of *BUS-SSAK* follows the same computational path as Kriging-based reliability analysis algorithms such as AK-MCS does [36]. However, there are two differences that are worth mentioning. First, the set of candidate design samples for Bayesian updating in the last step mainly comes from the local subset Ω_{m-1} but not the global sampling domain Ω, and the size of S_{m-1} is much smaller than the size of candidate design samples in AK-MCS. Second, as more failure (accepted) samples are generated in the last subset after the limit state $\hat{h}(\boldsymbol{x}) = 0$ is well constructed, the probabilistic property of the posterior distribution can be better inferred due to the sufficient information rendered by these samples. Main steps for the proposed Bayesian updating with subset simulation using Adaptive Kriging (*BUS-SSAK*) are summarized in Algorithm 4. Note that errors of $f'(\boldsymbol{x})$ mainly come from two sources. First, the surrogate limit state $\hat{h}(\boldsymbol{x}) = 0$ cannot be perfectly equal to the true performance function $h(\boldsymbol{x}) = 0$, which can unavoidably lead to wrong classification of acceptance and rejection. Second, the various settings of MCMC in the original framework (*BUS-SS*) regarding for example the jumping function can introduce error in the estimation of $f'(\boldsymbol{x})$. In the next section, the performance of the proposed method *BUS-SSAK* is explored by investigating three numerical examples.

Algorithm 4. Bayesian updating with subset simulation using adaptive Kriging (*BUS-SSAK*)

1. Generate N_{in} samples $\boldsymbol{x}_k, k = 1, \dots N_{in}$ using crude MCS and estimate their responses $h(\boldsymbol{x}_k), k = 1, \dots N_{in}$
2. $i = 1$
3. (a) If $i = 1$, identify t_1 using Algorithm 2 according to following steps:
    - **i**. Construct the Kriging model $\hat{h}_i(\cdot)$ based on current training samples $\boldsymbol{x}_{tr}$
    - **ii**. Build the Conditional Acceptance Rate Curve (CARC) according to Eq. (19)
    - **iii**. Search for $\hat{t}_1$ according to Eq. (20)
    - **iv**. Search for the next training point $\boldsymbol{x}_{tr}^*$ using dynamic learning function according to Eq. (31) and update the set of training samples $\boldsymbol{x}_{tr}$
    - **v**. Check if the stopping criterion is satisfied according to Eq. (32): if satisfied go to step 3 **vi**; Otherwise, estimate the response for $\boldsymbol{x}_{tr}^*$ and return to step 3 **i**.
    - **vi**. Output $\hat{t}_1$.

   (b) If $i > 1$, determine the intermediate acceptance rate t_k using Algorithm 2 such that the conditional acceptance rates satisfies $\mathrm{P}(\Omega_{i+1}|\Omega_i) \approx p_0$
4. Generate samples in Ω_i through crude MCS (if the probability of failure is not rare) or MCMC based on the remaining samples (i.e., seeds)
5. $i = i + 1$. Return to step 3 if $\hat{t} > 0$; otherwise, continue to step 6
6. Estimate the limit state $\hat{h}(\boldsymbol{x}) = 0$ according to following steps:
    - **i**. Generate candidate design samples S_{m-1} from the subset Ω_{m-1}
    - **ii**. Construct the Kriging model $\hat{h}_m(\cdot)$ based on current training samples $\boldsymbol{x}_{tr}$
    - **iii**. Estimate the mean $\sigma_{\hat{h}}(\boldsymbol{x})$ and standard deviation $\sigma_{\hat{h}}(\boldsymbol{x})$ for S_{m-1} with $\hat{h}_m(\cdot)$
    - **iv**. Search for the next best training samples $\boldsymbol{x}_{tr}^*$ using the learning function in Eq. (31), where $\hat{t} = 0$. Update the set of training samples $\boldsymbol{x}_{tr}$
    - **v**. Check if the stopping criterion is satisfied. Go to step 7, if it is satisfied; Otherwise, estimate the response $g(\boldsymbol{x}_{tr}^*)$ for $\boldsymbol{x}_{tr}^*$ and go back to Step 6 **iii**
7. Estimate the posterior distribution

4. Numerical Investigation

In this section, four examples are implemented to investigate the performance of the proposed method *BUS-SSAK*. The first example is tailored to showcase the implementation procedures of *BUS-SSAK*, while the rest of the examples are investigated to explore the computational performance compared to *BUS, aBUS*

[7] and *ANN-aBUS* [5] approaches. *aBUS* enhances the computational performance of *BUS* through adaptively adjusting the value of constant *c*, and therefore, does not need c as an input [7]. Moreover, *ANN-aBUS* integrates the *aBUS* algorithm with artificial neutral networks to substantially improve the computational performance of Bayesian model updating [5]. It should be noted that the time-complexity of the proposed method depends on the construction of the Kriging surrogate, which is in the order of $O(n^2)$ [46], [47]. The run time of the implemented codes is negligible compared to the run time of model evaluations. Therefore, the run time of the Bayesian updating methods is assessed using the number of model evaluations, N_{call}. Moreover, the accuracy of the proposed method has been investigated based on the ratio of estimated parameters through advanced techniques over the values estimated using MCS, e.g., $\hat{\mu}'/\mu'$ and $\hat{\sigma}'/\sigma'$. It should be noted that N_{ss} is the number of layers of subset, which is based on how rare the acceptance rate is. Moreover, N_{in} should be set sufficiently large so that the intermediate acceptance rate can be accurately identified. Based on several experiments performed in this study, $N_{in} = 5000$ can offer a reliable estimate of the posterior distribution for cases where the acceptance rate is larger than 10^{-6}. Moreover, N_t and N_{ts} can set to be very large due to the fact that generating samples in the accepted region is extremely fast using a well-trained Kriging surrogate model for the last subset.

4.1 Example 1: Illustration of methodology

The first example is implemented here to elaborate the implementation details of the proposed *BUS-SSAK* method . It investigates a one-dimensional problem where the random variable follows a standard normal prior distribution, denoted as $\varphi(x)$. The likelihood of this case follows a normal distribution with mean $\mu_l = 3$ and standard deviation $\sigma_l = 0.3$. And the maximum value of likelihood is $L_{max} = \frac{1}{\sigma_l\sqrt{2\pi}} = 1.33$, which means $c = \frac{1}{max(L_{max})} = 0.752$. Therefore, the reformulated limit state $h(x,p)$ can be written as:

$$h(x,p) = p - c\phi(x|\mu_l,\sigma_l) \quad (34)$$

where p is an auxiliary random variable following the standard uniform distribution and $\phi(\boldsymbol{x}|\mu_l,\sigma_l)$ denotes the probability density function of a normal distribution parameterized by μ_l and σ_l. To reduce the nonlinearity, the logarithmic formulation of the limit state function is used as follows [7]:

$$g(x,p) = ln(p) - ln(c) - ln\big(\phi(x|\mu_l,\sigma_l)\big) \quad (35)$$

In this example, the acceptance rate, P_{acc}, is 4.63×10^{-3}, which indicates that there are totally three subsets for the implementation of *BUS-SSAK*. The number of initial training samples is selected as 10. The performance of the considered methods is evaluated in terms of the number of calls to the likelihood function, N_{call} and ratios of the true and estimated mean and standard deviation of the posterior distribution (i.e., $\hat{\mu}/\mu'$ and $\hat{\sigma}'/\sigma'$).

The true/estimated limit states and training samples generated through *BUS-SSAK* in each subset are illustrated in Fig. 3. It can be observed that the estimated limit state in each subset is very close to the true one after applying CARC and DLF. Moreover, figures depicting the evolution of $\hat{h}(x,p) = 0$ with increasing training samples 10, 20, 30 and 40 are also shown in Fig. 4. One can observe that the limit state $\hat{h}(x,p) = 0$ gets increasingly close to $h(x,p) = 0$ as training samples increase. Consequently, the proposed approach, *BUS-SSAK*, can dramatically reduce the number of calls to the performance function to $N_{call} = 98$, while offering a high accuracy with $\frac{\hat{\mu}'}{\mu'} = 1.031$ and $\frac{\hat{\sigma}'}{\sigma'} = 0.9723$. The reason for the high computational efficiency is that the proposed method strategically calls the performance function to explore and refine the limit state.

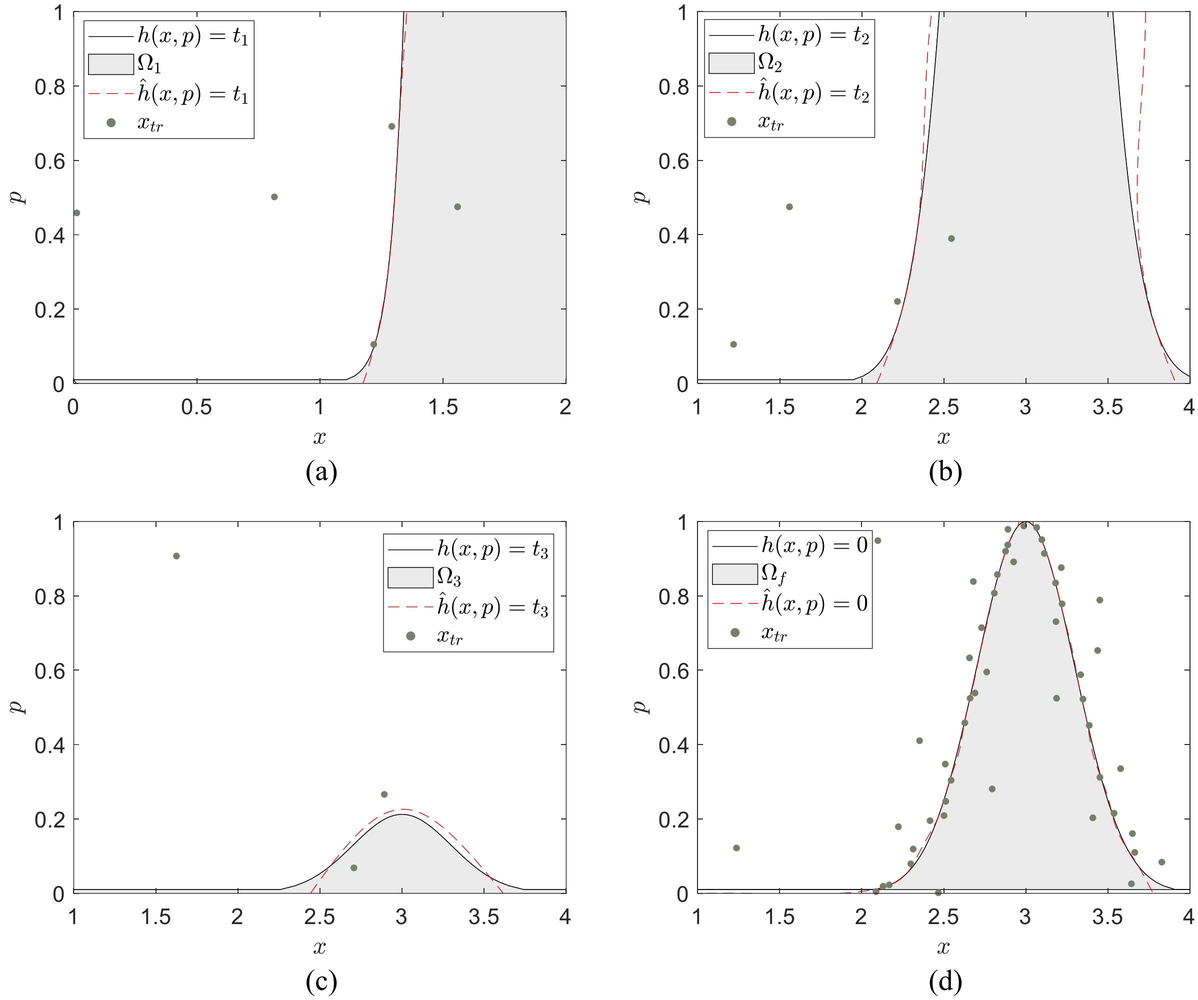

Fig. 3. Illustration of *BUS-SSAK* with the true/estimated limit states and training samples in (a) the first subset, (b) the second subset, (c) the third subset, and (d) the last subset.

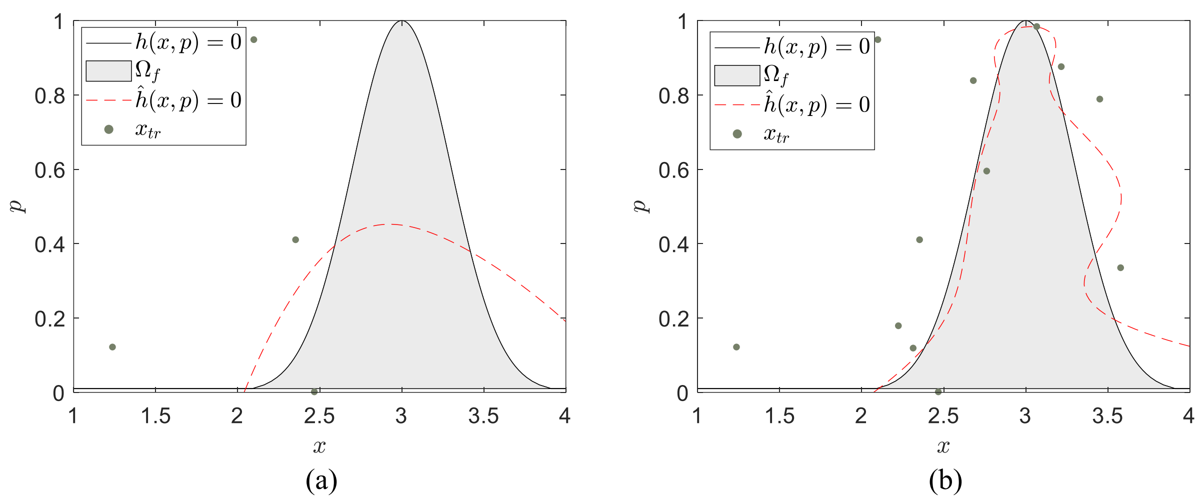

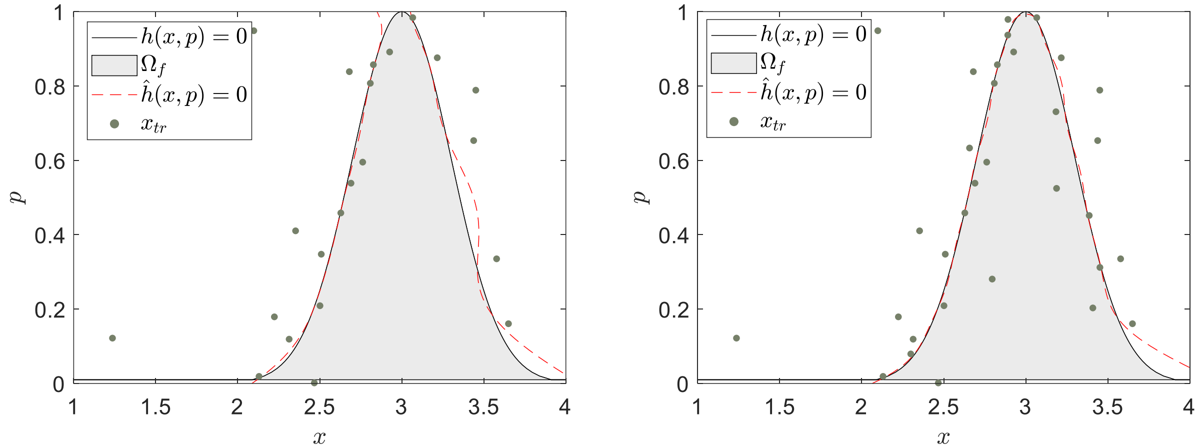

(c) (d)

Fig. 4. Illustration of $\hat{h}(x,p)=0$ with (a) 10 training samples, (b) 20 training samples, (c) 30 training samples, and (d) 40 training samples.

4.2 Example 2: Unimodal distribution

The first example concerns determining the posterior distribution in a problem with *n* random variables [5], [48]. First, the prior probability density function of the random variables can be represented as $f(\boldsymbol{x})=\prod_{i=1}^{n}\varphi(x_i)$, where $\varphi(\cdot)$ denotes the PDF of the standard normal distribution. Moreover, the likelihood function $L(\boldsymbol{x})$ can be represented as,

$$L(\boldsymbol{x})=\prod_{i=1}^{n}\frac{1}{\sigma_l}\phi(x_i|\mu_l,\sigma_l) \tag{36}$$

where σ_l is set as 0.2 and μ_l can be computed as follows,

$$\mu_l=\sqrt{-2(1+\sigma_l^2)\cdot ln\left[c_E^{1/n}\cdot\sqrt{2\pi\cdot\sqrt{1+\sigma_l^2}}\right]} \tag{37}$$

where c_E is the model evidence. In this paper, the case of $n=2$ and $c_E=10^{-4}$ is investigated. The analytical mean and standard deviation of the posterior of each mutually independent standard normal random variable $\boldsymbol{x}$ can be calculated as,

$$\mu'=\frac{\mu_l}{1+\sigma_l^2},\qquad \sigma'=\sqrt{\frac{\sigma_l^2}{1+\sigma_l^2}} \tag{38}$$

As suggested in [7], the logarithmic form of the likelihood function is computationally more efficient, thus, the equivalent limit state function can be expressed as,

$$h(\boldsymbol{x},p)=\ ln(p)-ln(c)-ln\big(L(\boldsymbol{x})\big) \tag{39}$$

For this example, the number of candidate design samples in each subset is set as 5000 (i.e., the size of S_{m-1} in Algorithm 3 is equal to 5000). Moreover, the initial number of training samples is set as 10. In this paper, the computational accuracy and efficiency of the considered methods are evaluated in terms of the estimated mean and standard deviation of the posterior distribution (i.e., $\hat{\mu}'$ and $\hat{\sigma}'$) and the number of evaluations to the performance function (i.e., N_{call}). Simulation results for the *BUS*, *aBUS* and *ANN-aBUS* together with the proposed *BUS-SSAK* method are summarized in Table 1. The parameters of *aBUS* is set exactly the same as *BUS*, and the number of training samples for each subset in *ANN-aBUS* is set as 100 for this example. For *ANN-aBUS*, the parameters of the three layers including input, hidden and output layers are optimized based on Levenberg-Marquardt optimization algorithm[5]. The acceptance ratio, P_{acc}, is equal to 2.451×10^{-5}, therefore 5 subsets should be generated in the *BUS+SS* algorithm. The analytical posterior mean and standard deviation are estimated as $\mu' = 2.659$ and $\sigma' = 0.1961$, respectively, according to Eq. (39). The convergence history of identifying intermediate acceptance rate (i.e., the intermediate failure thresholds in the equivalent reliability problem) $\hat{t}_i$ is shown in Fig. 5. Moreover, Fig. 6 illustrates the evolution of accepted candidate design samples through the *BUS-SSAK* approach. Fig. 7 showcases the process of adaptively enriching the set of training samples in each subset.

According to Table 1, the proposed *BUS-SSAK* approach is computationally very efficient and accurate. Essentially, the ratios between the estimated and true mean and standard deviation (i.e., $\hat{\mu}'/\mu'$ and $\hat{\sigma}'/\sigma'$) are computed as 1.018 and 1.009, while they are estimated as 1.007 and 1.051 via the *BUS+SS* method. However, the total number of evaluations of the likelihood function is only 34 for the proposed *BUS-SSAK* method while these numbers are 2838, 2643 and 603 for the *BUS+SS*, *aBUS* and *ANN-aBUS* approaches, respectively. This large number of function evaluations through *BUS* and *aBUS* poses a computational challenge for Bayesian updating of sophisticated models. Moreover, *BUS+SSAK* substantially overperforms *ANN-aBUS* due to the fact that the former approach selects training samples that are located in the vicinity of the limit state as opposed to the latter approach that tends to select training samples purely randomly. The intermediate acceptance rate $\hat{t}_i$, shown by dashed line in Fig. 5, asymptomatically converges to the true t_i shown by the solid line in Fig. 5. Specifically, $\hat{t}_1$ to $\hat{t}_4$ are identified 94.71, 31.24, 6.82 and -0.25 as shown in Fig. 5. Note that the number of subsets is 4, which is different with the one estimated through *BUS+SS* (i.e., 5). This is due to the variation of the MCMC technique applied in two algorithms, which determines the paths to the failure region but not the destination (failure region). However, it does not affect the training process of the Kriging model in the last subset, which plays an important role in determining the computational performance of *BUS+SSAK*. Moreover, according to Fig. 6(a), candidate design samples for the prior distribution are first generated by the MC sampling technique. Then, the initial training samples $\boldsymbol{x}_{in}$ are randomly selected from the first set of candidate design samples as shown in Fig. 7(a). Subsequently, the first intermediate $\hat{t}_1$ is accurately identified by Algorithm 2. In this process, new training samples are selected for the construction of the Kriging model as shown in Fig. 7(b). Repeating this process as presented in Algorithm 4, the candidate design samples are finally drawn for the last subset. Samples in the last subset follow the posterior distribution. From Fig. 6 and 7, it is evident that the training samples spread toward the final subset, which is also the acceptance (failure) region. This trend can also be explained by the two new concepts introduced in this paper. First, the estimated intermediate acceptance rate thresholds are adaptively identified to be smaller than zero. Second, the proposed dynamic learning function is applied to enrich the training set with samples that are close to the limit state $h(\boldsymbol{x}, p) = \hat{t}_i$. This approach tends to select samples that are close to the failure domain with extremely low probability density in the equivalent reliability problem. This process is adaptive so that the training samples are not passively selected beforehand, rather the training set is enriched sequentially based on the information provided by the responses of the likelihood function. This adaptive strategy can significantly improve the computational efficiency. In its current form, the process enriches one training point in each iteration. This means that the aggregated time of simulation is proportional to N_{call}. The computational time can be shortened by implementing appropriate parallel training strategies. Developing such strategies can be an important future research direction.

Table 1. Bayesian updating results of *BUS+SS* and *BUS-SSAK* for Example 1, where $\hat{\mu}'/\mu'$ and $\hat{\sigma}'/\sigma'$ denote the estimated/true means and standard deviations of the posterior distribution.

Methodology	N_{call}	$\hat{\mu}'$	$\hat{\sigma}'$	$\hat{\mu}'/\mu'$	$\hat{\sigma}'/\sigma'$
BUS+SS	2838	2.6765	0.2061	1.007	1.051
aBUS	2634	2.695	0.1949	1.000	0.994
ANN-aBUS	603	2.6643	0.1867	1.002	0.952
BUS-SSAK	$10 + 24$	2.7067	0.1978	1.018	1.009

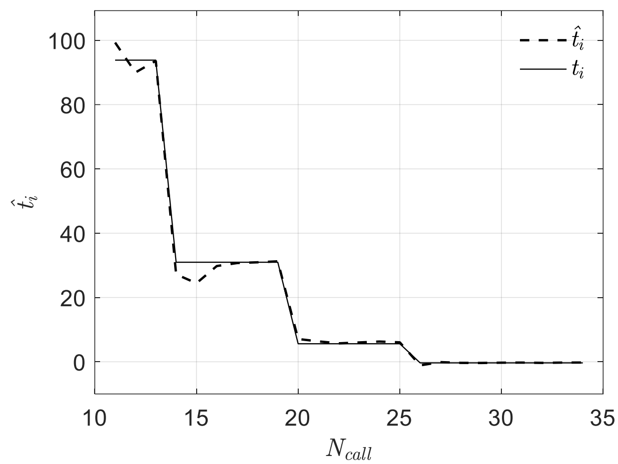

Fig. 5. Convergence history of identifying $\hat{t}_i$ till $\hat{t}_i \leq 0$.

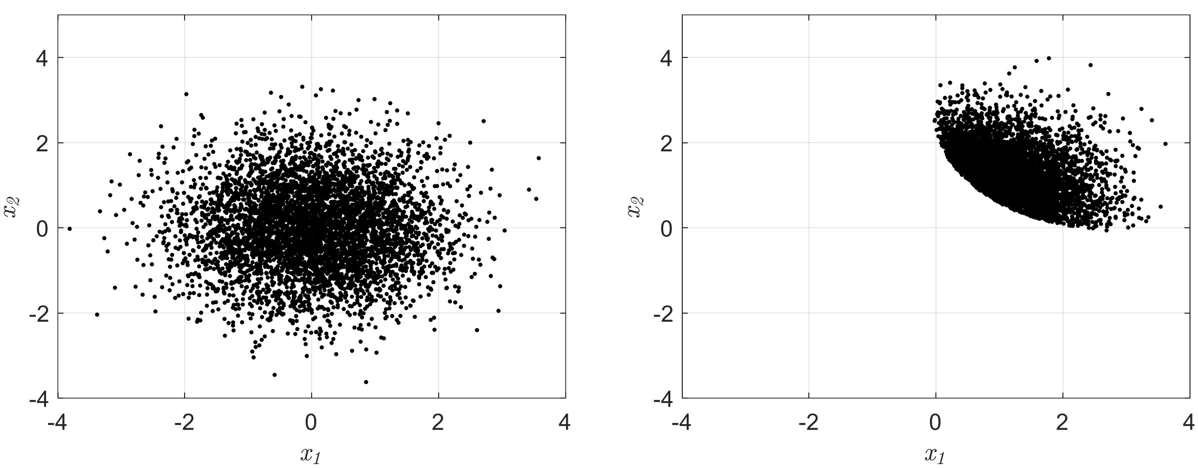

(a) MC samples (b) *BUS-SSAK* samples in subset 1

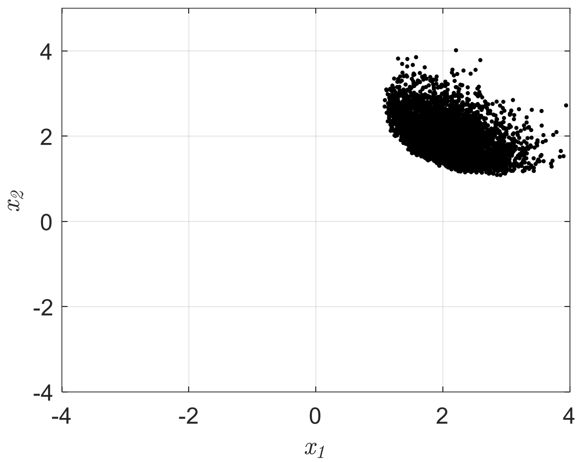

(c) *BUS-SSAK* samples in subset 2

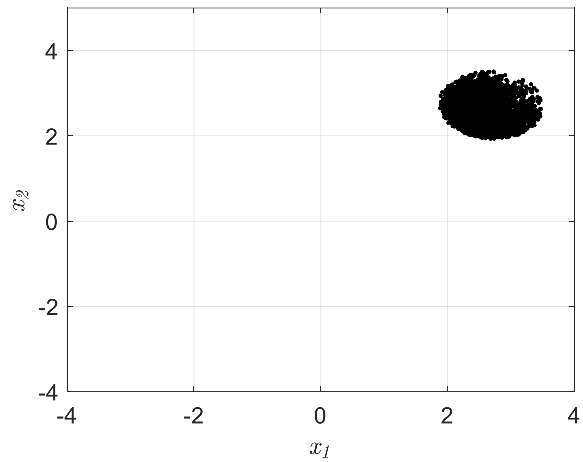

(d) *BUS-SSAK* samples in subset 3

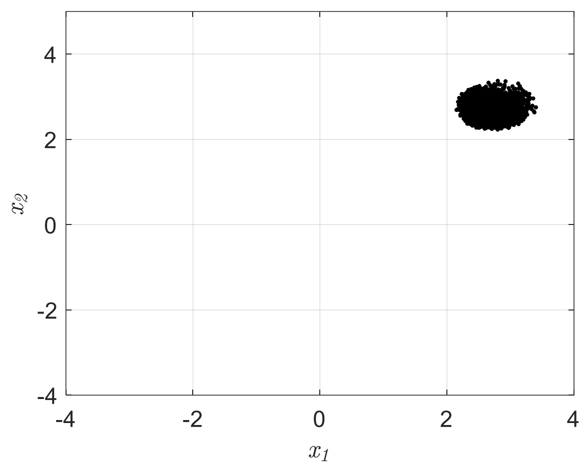

(e) *BUS-SSAK* samples in the final subset

Fig. 6. Simulation Results of *BUS-SSAK* with accepted samples in each subset.

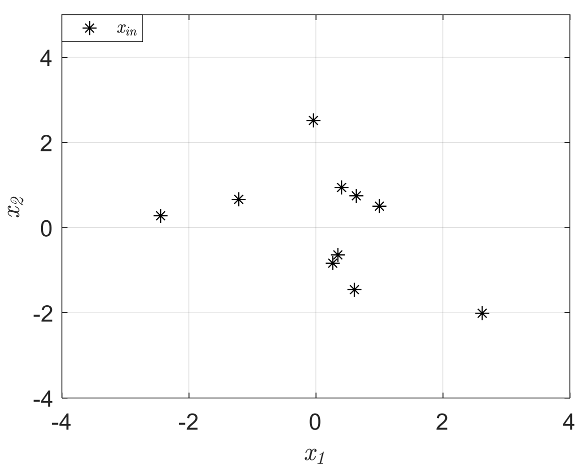

(a) Initial training samples

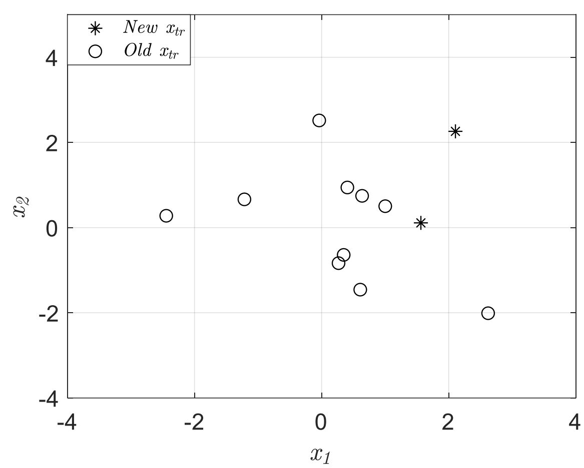

(b) Training samples in subset 1

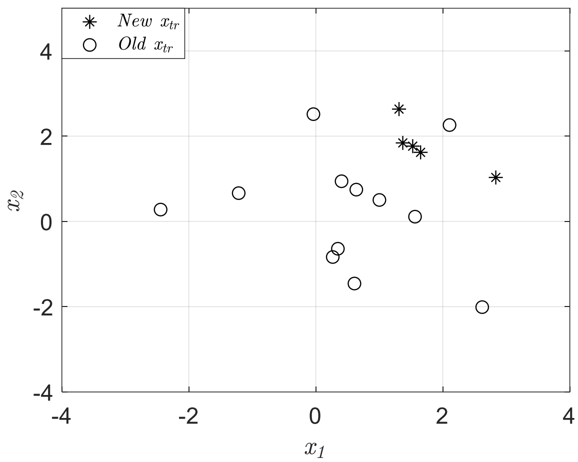

(c) Training samples in subset 2

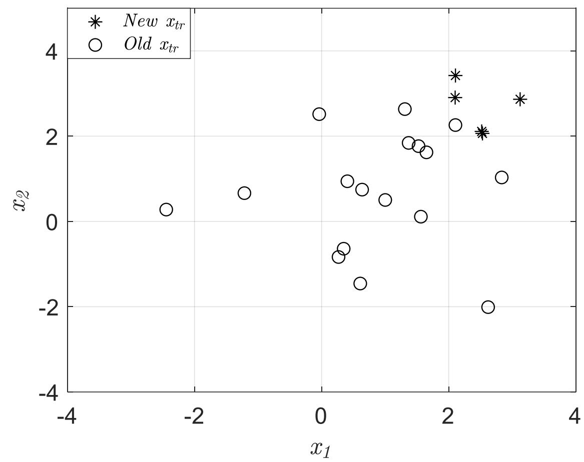

(d) Training samples in subset 3

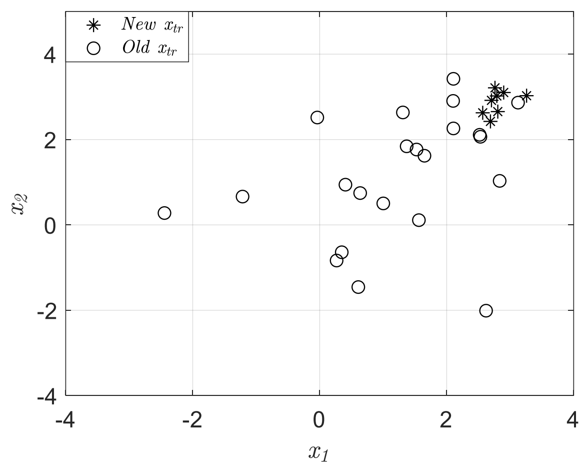

(e) Training samples in the final subset

Fig. 7. Simulation results of *BUS-SSAK* with training samples in each subset.

4.3 Example 3: Two degrees-of-freedom structure

The second example involves a two-degrees-of-freedom (two-DOF) dynamic system which was developed in [4] and then investigated in [5]–[7] to explore the performance of *BUS*. By measuring the eigen-frequencies of the structure, the posterior distribution of inter-story stiffnesses is estimated using the Bayesian updating technique. Fig. 8 illustrates the configuration of this structure. The masses of the two stories are defined as $m_1 = 16.531 \cdot 10^3\ kg$ and $m_2 = 16.13.1 \cdot 10^3\ kg$. The inter-story stiffnesses are modeled as $K_1 = X_1 k_n$ and $K_2 = X_2 k_n$, where K_1 and K_2 are the stiffness values of the first and second stories, respectively, $k_n = 29.7 \cdot 10^6\ N/m$ is the nominal value, and X_1 and X_2 are correction factors to be updated. Damping is not considered in this case. Observations of the first two eigen-frequencies f_1 and f_2 are used to update the distribution of $\boldsymbol{X} = [X_1, X_2]$. According to [4], [6], the likelihood function for this problem can be expressed as,

$$L(\boldsymbol{x}) \propto \exp\left[-\frac{J(\boldsymbol{x})}{2\sigma_\varepsilon^2}\right] \qquad (40)$$

where

$$J(\boldsymbol{x}) = \sum_{j=1}^{2} \lambda_j^2 \left[\frac{f_j^2(\boldsymbol{x})}{\tilde{f}_j^2} - 1 \right]^2 \tag{41}$$

is a measure-of-fit function. $f_j^2(\boldsymbol{x})$ is the *j*th eigen-frequency estimated from the structural model with random variables $\boldsymbol{x}$, and $\tilde{f}_j^2$ is the measurement of the *j*th eigen-frequency. $\lambda_1 = \lambda_2 = 1$ are the means and $\sigma_\varepsilon = \frac{1}{16}$ is the standard deviation of the prediction error. Two measurements of eigen-frequencies are available: $\tilde{f}_1 = 3.13$ Hz and $\tilde{f}_2 = 9.83$ Hz. However, one should note that the parameters of the structures can be also updated based on the data allow inferring about the mode shapes or a combination of data on frequency and mode shapes. Moreover, the present study assumes that the structure is not damaged. In the case where the structure is damaged, the mode-switching problem may emerge as the loss of stiffness in structural elements may unevenly impact some of the modal frequencies more than others and therefore switch the order of the modes. More information about this issue can be found in [49]. The prior distribution of X_1 and X_2 are uncorrelated lognormal distributions with modes 1.3 and 0.8 and standard deviations $\sigma_{X_1} = \sigma_{X_2} = 1$.

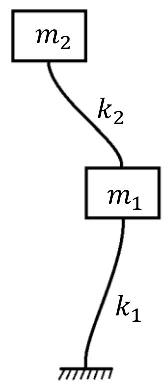

Fig. 8. Two-DOF shear building model.

The limit state function can be rewritten as,

$$h(\boldsymbol{x}, p) = p - c \cdot \exp\left[-\frac{J(\boldsymbol{x})}{2\sigma_\varepsilon^2} \right] \tag{42}$$

The acceptance rate of the undecomposed limit state function in Eq. (42) is approximately 0.0016; therefore, three subsets are needed to implement *BUS*. Similar to the previous examples, the logarithmic form of Eq. (42) is used here. N_{in} and the initial number of training samples are set as 5000 and 10, respectively. The *BUS+SS*, *aBUS*, *ANN-aBUS* and the proposed *BUS-SSAK* methods are implemented to assess their performance for this example. The results are summarized in Table 2. The parameters of aBUS are set the same as *BUS*, and the number of training samples for each subset in *ANN-aBUS* is set as 300 for this example. Fig. 9 illustrates the convergence of $\hat{t}_i$ to the true rate. Moreover, the evolution of the set of accepted candidate design samples in the *BUS-SSAK* method is shown in Fig. 10. In addition, Fig. 11 showcases the evolution of the set of training samples in each subset. According to Table 2, the mean and standard deviation of the estimated $f'(x)$ via *BUS+SS* and *BUS-SSAK* are close $\Delta_{\hat{\mu}'(L)} = (0.499 - 0.497)/0.499 = 0.004$, $\Delta_{\hat{\mu}'(R)} = (1.832 - 1.819)/1.832 = 0.0071$, $\Delta_{\hat{\sigma}'(L)} = (0.038 - 0.035)/0.038 = -0.0789$ and $\Delta_{\hat{\sigma}'(R)} = (0.140 - 0.134)/0.140 = 0.0429$. However, the total number of evaluations of the likelihood function is only 151 for the proposed *BUS-SSAK* method compared to 3432, 3165, 2447 evaluations for *BUS+SS*, *aBUS* and *ANN-aBUS*, respectively. Moreover, the posterior parameters estimated through *BUS-SSAK* are found to be more accurate than *ANN-aBUS*. Approximately 120, 13, and 18 evaluations of the likelihood function are used in subsets 1, 2, and 3 via *BUS+SS*, respectively, according to Fig. 9. Specifically, $\hat{t}_1$ to $\hat{t}_3$ are identified 32.3, 3.94 and -1.22 as shown in Fig. 12. Comparing Fig. 10 and 11, one can find that the new training samples are strategically added in the area located in the final subset in Fig. 11(d). Therefore, the computational accuracy and efficiency of the proposed method are demonstrated for the three considered examples.

Table 2. Bayesian updating results for example 2.

Methodology	N_{call}	$\hat{\mu}'(L)$	$\hat{\sigma}'(L)$	$\hat{\mu}'(R)$	$\hat{\sigma}'(R)$
BUS+SS	3432	0.497	0.038	1.819	0.140
aBUS	3165	0.499	0.040	1.821	0.141
ANN-aBUS	2447	0.487	0.033	1.837	0.127
BUS-SSAK	10+ 131	0.499	0.035	1.832	0.134

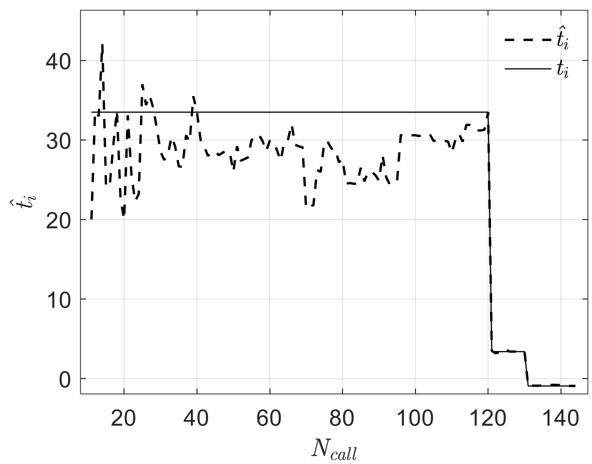

Fig. 9. Convergence history of identifying $\hat{t}_i$ till $\hat{t}_i \leq 0$.

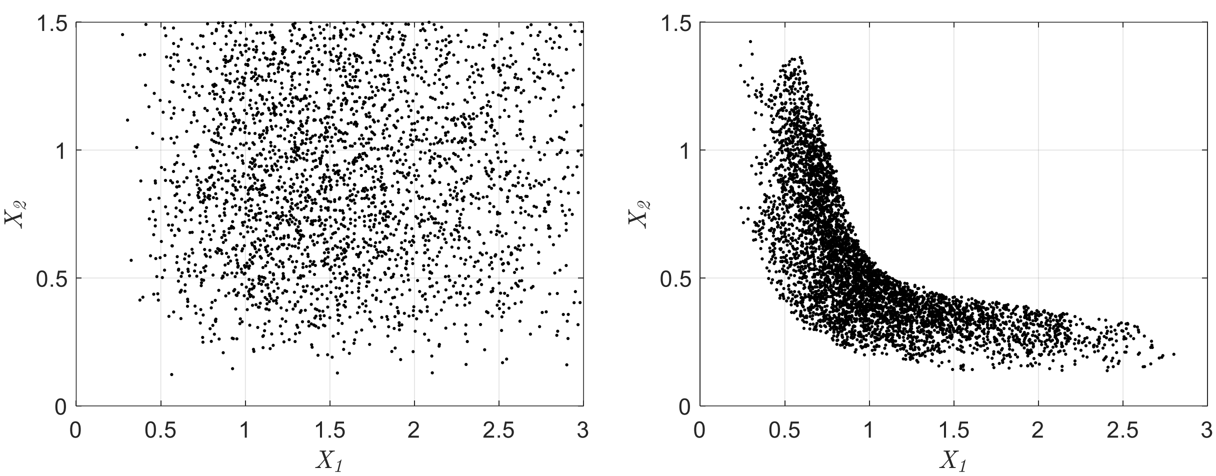

(a) MC samples (b) *BUS-SSAK* samples in subset 1

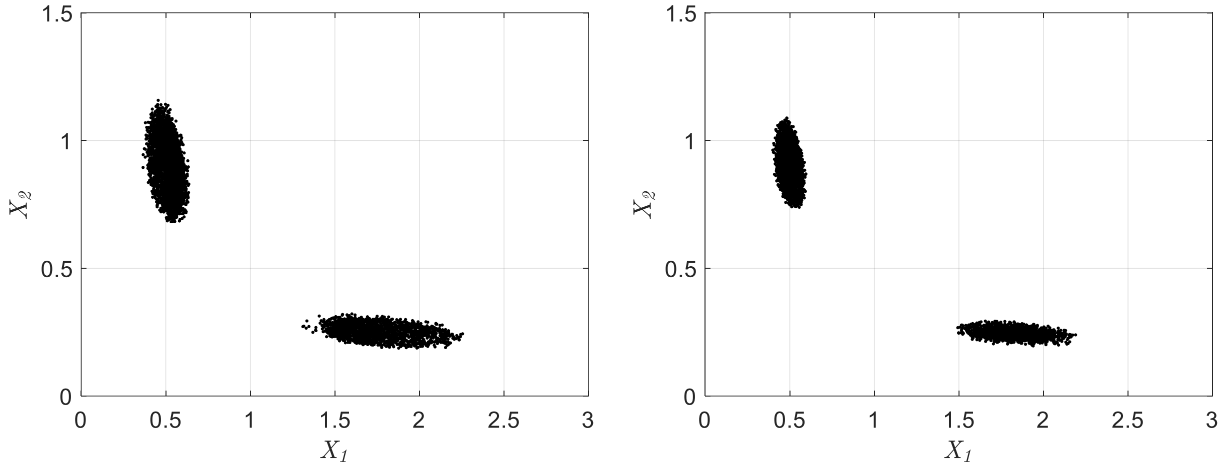

(c) *BUS-SSAK* samples in subset 2 (d) *BUS-SSAK* samples in the final subset

Fig. 10. Simulation results of *BUS-SSAK* with accepted samples in each subset

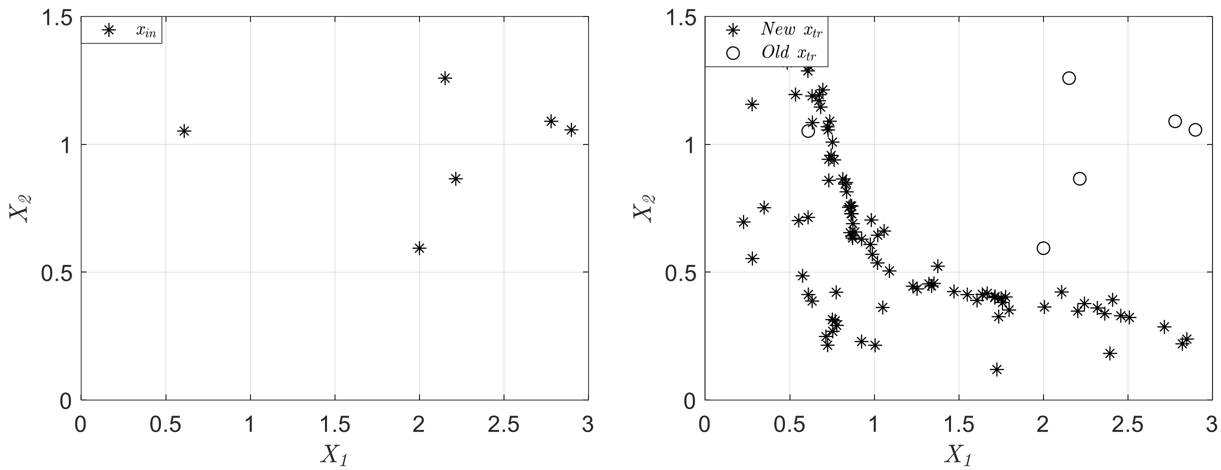

(a) Initial training samples (b) Training samples in subset 1

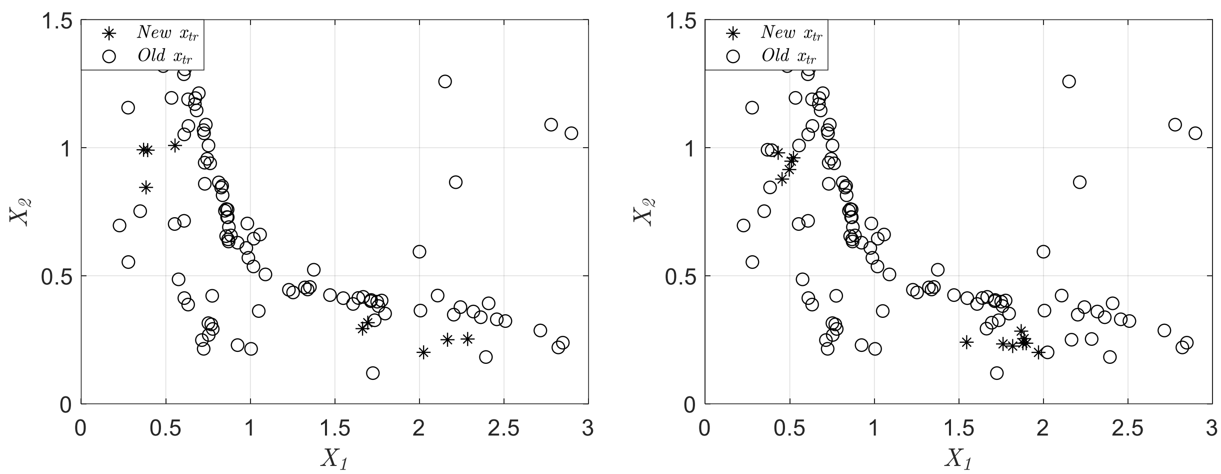

(c) Training samples in subset 2 (d) Training samples in the final subset

Fig. 11. Simulation Results of *BUS-SSAK* with training samples in each subset.

4.4 Example 4: A model of chloride and carbonation-based corrosion

This section investigates the computational performance of the proposed surrogate-based Bayesian updating approach for an engineering application related to durability modeling for chloride corrosion. The mechanism of chloride ingress in a partially carbonated concrete medium is first introduced followed by the modeling process that is based on the finite difference method. Finally, the derivation of the posterior distributions of model parameters using the proposed *BUS-SSAK* method is presented for the case where two observations for chloride concentration and carbonation depth are available.

4.4.1 Model description

Engineered structures such as cross-sea bridges are exposed to highly corrosive environments. Durability of these structures that are often made of concrete against deterioration processes such as chloride and carbonation-induced corrosions is one of the most challenging issues for life-cycle management. As shown in Fig**.** 12, the tidal zones of the concrete columns of the cross-sea suspension bridge are subject to simultaneous deterioration by chloride corrosion and carbonation. The darker dots in Fig. 12 represent chloride ions, while the brighter dots indicate carbon dioxide.

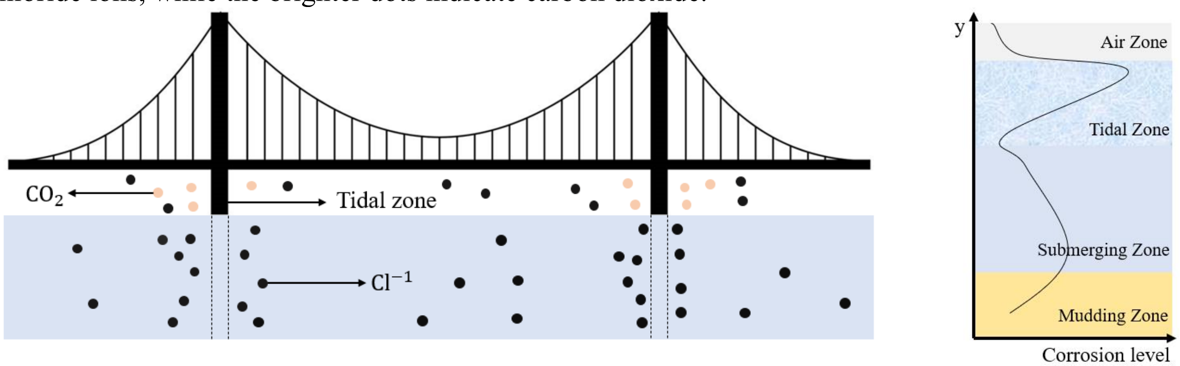

(a) (b)

Fig. 12. A suspension bridge in marine environment: (a) A conceptual plot of the bridge and the corrosive environment and (b) Corrosion profile for different zones

Through diffusion across carbonated and uncarbonated regions of concrete, chloride ions ingress the protective layer of concrete located in the submerging zone and reach the surface of the very exterior steel reinforcement in concrete elements. The subsequent chemical reactions of chloride with steel can significantly affect the functionality of concrete structures during their service life. Chloride transport is typically described by the Fick's second law, which can be represented by the following partial differential equations,

$$\frac{\partial C_{cl}}{\partial t} = D_1 \frac{\partial^2 C_{cl}}{\partial x^2}, 0 \leq x \leq L_c$$

$$\frac{\partial C_{cl}}{\partial t} = D_2 \frac{\partial^2 C_{cl}}{\partial x^2}, x > L_c \tag{43}$$

where C_{cl} denotes chloride concentration, D_1 and D_2 are the two diffusion coefficients of uncarbonated and carbonated regions and L_c denotes the depth of the carbonation, which can be calculated as follows,

$$L_c = k_c \sqrt{t_c} \tag{44}$$

where k_c denotes the carbonation coefficient and t_c denotes the time (year). A conceptual illustration of chloride diffusion process is shown in Fig**.** 13. The initial and boundary conditions for the above partial differential equations are as follows,

$$
\begin{aligned}
C_{cl}(t_c = 0) &= c_0, \\
C_{cl}(x = 0, t_c > 0) &= c_s > c_0, \\
C_{cl}|_{x=L_C^-} &= C_{cl}|_{x=L_C^+}, \\
D_1 \frac{\partial C_{cl}}{\partial x}|_{x=L_C^-} &= D_2 \frac{\partial C_{cl}}{\partial x}|_{x=L_C^+}
\end{aligned}
\tag{45}
$$

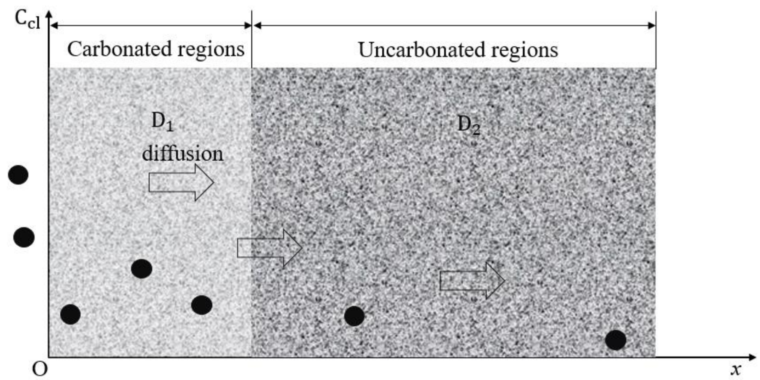

Fig. 13. Illustration of chloride transport in partially carbonated concrete. Dark circles indicate chloride ions.

The corrosion model of Eq.(43) is solved using finite difference method. It should be noted that this approach and the proposed Bayesian updating method can be applied to any type of diffusion-based corrosion simulation such as those involving convection with pore solution flow.

4.4.2 Finite difference discretization

The diffusion process of chloride ions in partially carbonated concrete can be simulated using finite difference method through the following discretization,

$$
\frac{C_{cl}^{i,j+1} - C_{cl}^{i,j}}{\Delta t} = D_{cl} \frac{C_{cl}^{i,j+1} - 2C_{cl}^{i,j} + C_{cl}^{i,j-1}}{\Delta x^2}, 0 \leq x \leq L_c
$$

$$
\frac{C_{cl}^{i,j+1} - C_{cl}^{i,j}}{\Delta t} = D_{cl} \frac{C_{cl}^{i,j+1} - 2C_{cl}^{i,j} + C_{cl}^{i,j-1}}{\Delta x^2}, x > L_c \tag{46}
$$

The explicit formulation of finite difference is adopted in this paper due to its computational simplicity. Based on Eq.(45), the specific initial conditions for this problem are defined as $C_{cl}^{i,0} = c_0$, $C_{cl}^{0,j>0} = c_s > c_0$ and $C_{cl}^{\infty,0} = 0$, where $c_0 = 0$ and $c_s > 0$ denote the surface chloride concentration and the value of C_{cl} at initial time $t_c = 0$. Moreover, parameters for finite difference discretization, i.e. Δx and Δt are set as 0.0001m and 0.05 year, respectively. An illustration of the finite difference discretization and chloride concentration, C_{cl} at $t_c = 20$ years are presented in Fig. 14. The time for one simulation is about 10.21 seconds.

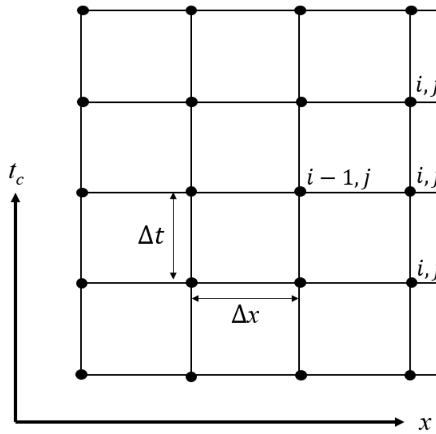

(a) finite difference discretization in 2D

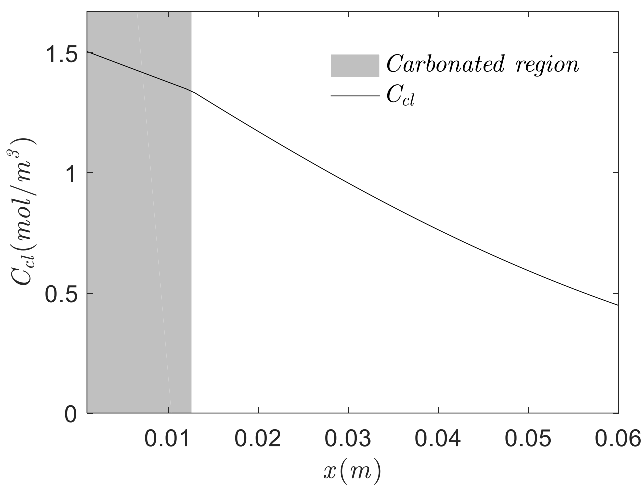

(b) chloride concentration with $t_c = 20$ years, where the gray region is the carbonated part of concrete

Fig. 14. Illustrations of chloride and carbonation-based corrosion using finite difference method

4.4.3 Results of Bayesian updating

This subsection showcases the computational process to infer the posterior distribution of chloride concentration and carbonation depth based on the observed data using the proposed method. The prior distributions of four parameters including c_s, D_1, D_2 and k_c are summarized in Table 3. An agency in charge of bridge management plans to estimate the posterior distribution of C_{cl} and k_c based on field observations in support of decisions for future maintenance and inspection. Note that knowing the distribution of k_c, one can determine the distribution of L_c using Eq.(44). A concrete sample is taken from the tidal zone of a bridge column and analyzed using Volhard's Titration Method to determine C_{cl} and L_c at $t_c = 5$ years. Analysis of the specimen yielded $C_{cl}|_{x=0.005,t_c=5} = 1.823$ mol/m^3 and $L_c|_{x=0.005,t_c=5} =$ 0.0057 m. The errors associated with these measurements are modeled with ε_{m1}, a normal distribution with mean 0 and standard deviation 0.05, and ε_{m2}, a normal distribution with mean 0 and standard deviation 0.0005, respectively. Thus, the likelihood function can be represented as:

$$L(\boldsymbol{x}) = \varphi_1(\varepsilon_{m1}) \cdot \varphi_2(\varepsilon_{m2}) = \varphi_1\left(1.823 - C_{cl}|_{x=0.005,t=5}\right) \cdot \varphi_2\left(0.0057 - L_c|_{x=0.005,t=5}\right)$$

where φ_1 is the PDF of a normal distribution with mean 0 and standard deviation 0.05 and φ_2 is the PDF of a normal distribution with mean 0 and standard deviation 0.0005. The limit state function for the *BUS* approach can be rewritten as,

$$h(\boldsymbol{x}, p) = p - cL(\boldsymbol{x}) \tag{48}$$

By taking the logarithmic form of Eq.(48), a mathematically equivalent but simpler linear form of the equation can be derived as:

$$h(\boldsymbol{x}, p) = ln(p) - ln(c) - ln\big(L(\boldsymbol{x})\big) \tag{49}$$

Simulation results are presented in **Fig.** 15. Specifically, **Fig**. 15(a) showcases the convergence history of the identified intermediate acceptance rate with the solid line denoting the true value and the dashed line denoting the dynamically estimated quantity. Moreover, the evolution of parameters c_s and k_c from prior to posterior distributions are plotted in **Fig.** 15(b). **Fig.** 15(c) shows the modes and 95% confidence intervals (CIs) for the prior and posterior distribution of C_{cl} at time $t_c = 50$ years along the concrete protective depth $x \in [0,0.05]$ m. In this figure, the red/black solid lines denote the mode of posterior/prior distribution of C_{cl} with yellow/gray shadow regions representing 95% CIs. Moreover, the modes and 95% confidence intervals for prior and posterior distribution of C_{cl} at location $x = 0.05$ in the period of $t_c \in [0,50]$ years are plotted in **Fig.** 15(d). The proposed *BUS-SSAK* algorithm converges with 199 evaluations of the finite difference-based chloride ingress model and the total simulation time of $\mathrm{T_s} = 10.21\ \mathrm{s} \times 199 = 2032$ seconds. Without the proposed *BUS-SSAK* method, *BUS* will take more than $10.21\ \mathrm{s} \times 1500 = 4.25h$. Therefore, it significantly improves the computational efficiency for this relatively simple corrosion benchmark problem. This efficiency can be more distinct as the FEM becomes more sophisticated. Moreover, the simulation time for estimating posterior distribution for those parameters through other approaches such as *BUS-SS*, *aBUS* and *ANN-aBUS* are prohibitively large. Therefore, the proposed algorithm enables estimation of the posterior distribution of properties even when complex models and simulations are involved.

Table 3. Prior distribution of parameters.

Random variable	Distribution	Mean	C.O.V
c_s	Lognormal	1.52[mol/m^3]	0.1
D_1	Lognormal	2.5×10^{-4}[m^2/y]	0.1
D_2	Lognormal	1.5×10^{-4}[m^2/y]	0.1
k_c	Lognormal	0.004 [m/y$^{1/2}$]	0.1

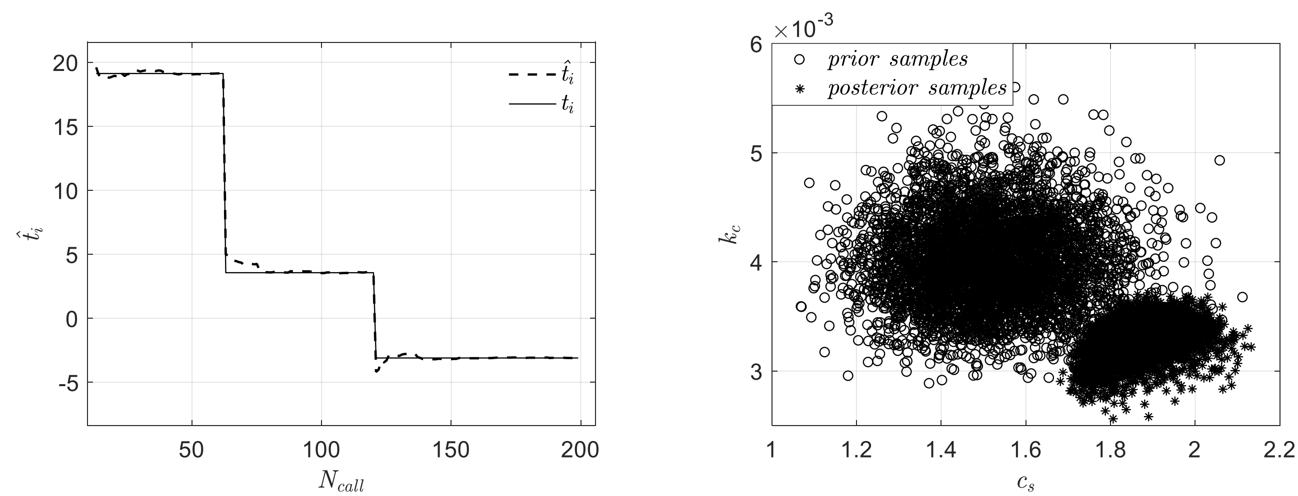

(a) *(b)*

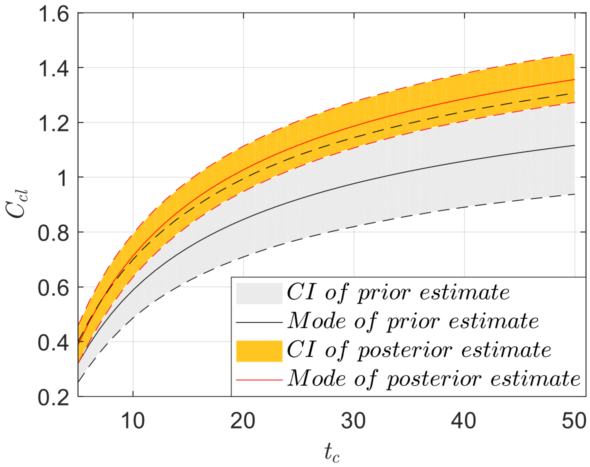

(c)

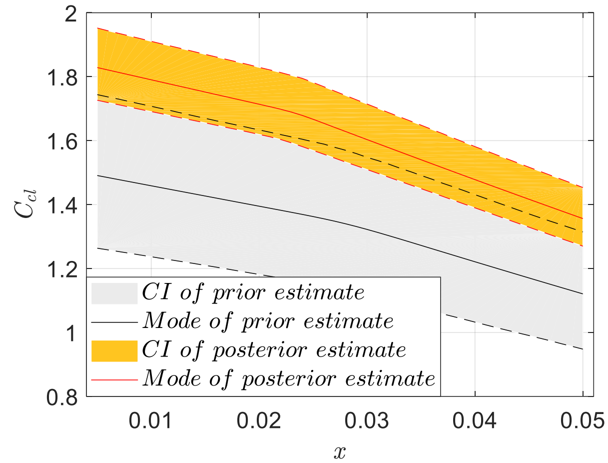

(d)

Fig. 15. Illustrations of results of Example 3 using the proposed method: (a) the convergence history of identified intermediate failure thresholds; (b) the evolution of samples from prior to posterior distribution based; (c) modes and 95% CIs for prior and posterior estimates of C_{cl} at location $x = 0.05$ m in the period of $t_c \in [0,50]$ years; and (d) modes and 95% CIs for the prior and posterior estimates of C_{cl} at time $t_c =$ 50[year] along the concrete protective depth $x \in [0,0.05]$ m

5. Conclusion

This paper proposes a new approach to Bayesian updating called *BUS-SSAK*, to improve the computational efficiency of estimating the posterior distribution of random variables and enable Bayesian updating for complex computational models. Generally, the main idea behind *BUS-SSAK* is to identify the sampling seeds of MCMC located in the final accepted domain. Two concepts are introduced to enable this process: Conditional Acceptance Rate Curve (CARC) and Dynamic Learning Function (DLF). CARC is a model that relates the value of intermediate failure threshold to intermediate failure probability as well as the corresponding confidence interval. DLF is a learning model that enables strategically adding training samples in the vicinity of the equivalent limit state with intermediate failure thresholds. After the seeds located in the accepted domain are accurately captured, Kriging-based reliability analysis methods are implemented to train the surrogate model for the equivalent limit state function reinterpreted by *BUS*. The final accepted samples following the posterior distribution are generated by implementing the MCMC sampling based on aforementioned seeds and the well-trained Kriging surrogate model. Three examples are investigated in this paper. Compared to the approach via the combination of *BUS* and pure subset simulation (*BUS+SS*), the proposed *BUS-SSAK* method significantly reduces the computational cost by one to two orders of magnitude and simultaneously maintain high accuracy in the estimate of posterior distributions.

Despite the significant computational advancements offered by the proposed method, it can be further enhanced in the future. First, the proposed method, similar to other techniques, can face high computational demands as the dimension of the problem, i.e., the number of random variables becomes very large. This is in part due to the inherent shortcomings of Kriging surrogate models when facing the challenge of curse of dimensionality. Moreover, advanced stopping criteria that can associate termination of active training to error in posterior estimation can avoid costs of unnecessary training or risks of premature termination.

Appendix 1: Algorithms of subset simulation and *BUS-SS*

Algorithm 1A. Subset simulation for failure probability estimation

1. Generate N_{SS} samples $\boldsymbol{x}_k, k = 1, \dots N_{SS}$ through crude MCS and estimate their responses $g(\boldsymbol{x}_k), k = 1, \dots N_{SS}$
2. $i = 1$
3. (a) If $i = 1$, determine t_1 such that $\mathrm{P}(\Omega_1) \approx p_0$

(b) If $i > 1$, determine the intermediate failure thresholds t_is such that the conditional probabilities satisfy $\mathrm{P}(\Omega_{i+1}|\Omega_i) \approx p_0$
4. Generate samples in Ω_{i+1}(i.e., if the probability of failure is not rare, pure MCS is recommended; otherwise, MCMC is appropriate)
5. $i = i + 1$. Return to step 3 if $t_i > 0$; otherwise, continue to step 6.
6. Estimate the last failure probability $\hat{P}_0^m = \mathrm{P}(\Omega_m|\Omega_{m-1})$ in the final subset $\Omega_m$with $t_m = 0$
7. Estimate the failure probability $\hat{P}_f^{ss}$ according to Eq. (16).

Algorithm 1B. *BUS* with Subset simulation

1. Define the parameters:
   (a) Target number of samples N_t
   (b) Number of samples in each intermediate step N_{in}
   (c) Probability of intermediate subsets p_0
   (d) Constant c according to Eq. (9)
2. Draw N_{in} samples $[\boldsymbol{x_k}, p_k], k = 1,2, \dots N_{in}$ from the prior distribution $[\boldsymbol{X}, P]$
3. Define the subset domain such that $\Omega_1 = \{h(\boldsymbol{x}, p) \leq t_1\}$, where t_1 is defined according to the p_0 percentile of the responses of samples $h(\boldsymbol{x_k}, p_k), k = 1,2, \dots N_{in}$
4. $i = 1$
5. While $t_i > 0$,
   (a) $i = i + 1$
   (b) Draw N_{in} samples from the domain Ω_{i-1} with MCMC technique
   (c) Define the next subset $\Omega_i = \{h(\boldsymbol{x}, p) \leq t_i\}$, where t_i is defined according to the p_0 percentile of the responses of samples $h(\boldsymbol{x_k}, p_k), k = 1,2, \dots N_{in}$ in subset Ω_{i-1}
6. Define the last subset $\Omega_{i+1} = \{h(\boldsymbol{x}, p) \leq 0\}$, identify the number of samples N_s in Ω_{i+1} and keep these samples as seeds
7. Draw N_t samples in the subset Ω_{i+1} with those seeds in Step 6 using MCMC technique

Appendix 2: Elements of Kriging Model

The Kriging model, also called Gaussian Process Regression, makes a prior assumption that the estimated response $\hat{y}(\boldsymbol{x})$ and the known true response y follow a joint Gaussian distribution [24], [50], [51]. It has been widely used for surrogate-based reliability analysis [40], [52]–[56]. Based on this assumption, Kriging combines the process of interpolation and regression. The estimated stochastic response $K(\boldsymbol{x})$ for input $\boldsymbol{x}$ can be described as follows,

$$\boldsymbol{K}(\boldsymbol{x}) = \boldsymbol{\beta}^T \boldsymbol{f}_k(\boldsymbol{x}) + \boldsymbol{Z}_k(\boldsymbol{x}, \boldsymbol{w}) \tag{A1}$$

where $\boldsymbol{f}_k(\boldsymbol{x})$ is the basis function and $\boldsymbol{\beta}$ is the vector of regression coefficients of $\boldsymbol{f}_k(\boldsymbol{x})$. $\boldsymbol{\beta}^T \boldsymbol{f}_k(\boldsymbol{x})$ represents the mean value of $\boldsymbol{K}(\boldsymbol{x})$, which is often assumed to have ordinary (β_0), linear (β_0+$\sum_{i=1}^{N} \beta_i \boldsymbol{x}_i$) or quadratic ($\beta_0$+$\sum_{i=1}^{N} \beta_i \boldsymbol{x}_i$+$\beta_0$+$\sum_{i=1}^{N} \sum_{j=i}^{N} \beta_{ij} \boldsymbol{x}_i \boldsymbol{x}_j$) forms, where *N* is the dimension of the random input vector $\boldsymbol{x}$. More details on $\boldsymbol{f}_k(\boldsymbol{x})$ and $\boldsymbol{\beta}$ in Kriging models can be found in [51]. In this study, the ordinary Kriging model is used, meaning that both $\boldsymbol{f}_k(\boldsymbol{x})$ and $\boldsymbol{\beta}$ are constant. $\boldsymbol{Z}_k(\boldsymbol{x})$ is a stationary normal Gaussian process with zero mean and the following covariance matrix,

$$COV\big(\boldsymbol{Z}_k(\boldsymbol{x}), \boldsymbol{Z}_k(\boldsymbol{w})\big) = \sigma^2 \boldsymbol{R}(\boldsymbol{x}, \boldsymbol{w}, \boldsymbol{\theta}) \tag{A2}$$

where $\boldsymbol{x}$ and $\boldsymbol{w}$ are two arbitrary samples, and σ^2 is the process variance, which represents the generalized mean square error in the regression process. Moreover, $\boldsymbol{R}(\boldsymbol{x}, \boldsymbol{w}, \boldsymbol{\theta})$, called the kernel function, represents the correlation function of the process with hyper-parameter $\boldsymbol{\theta}$. A set of correlation functions have been implemented in Kriging including, but not limited to, linear, exponential, Gaussian and Matérn functions.

In this article, the separable anisotropic Gaussian function is used which has the following form,

$$\boldsymbol{R}(\boldsymbol{x},\boldsymbol{w},\boldsymbol{\theta}) = \prod_{i=1}^{N} \exp(-\boldsymbol{\theta}_i(\boldsymbol{x}_i - \boldsymbol{w}_i)^2) \tag{A3}$$

The hyper-parameter $\boldsymbol{\theta}$ can be determined using methods such as Maximum Likelihood Estimation (MLE) or Cross-Validation (CV) [51], among others. Here, $\boldsymbol{\theta}_i$ is found using MATLAB optimization toolbox DACE [57], [58] that uses the MLE method. The Maximum Likelihood Estimation approach is described below,

$$\boldsymbol{\theta} = \operatorname*{argmin}_{\theta^* \in \Theta} \left(|\boldsymbol{R}(\boldsymbol{x},\boldsymbol{w},\boldsymbol{\theta})|^{\frac{1}{m}} \sigma^2 \right) \tag{A4}$$

In the Kriging model, the regression coefficient $\boldsymbol{\beta}$ and the estimated mean response and variance can be determined as follows,

$$\boldsymbol{\beta} = (\boldsymbol{F}^T\boldsymbol{R}^{-1}\boldsymbol{F})^{-1}\boldsymbol{F}^T\boldsymbol{R}^{-1}\boldsymbol{y} \tag{A5}$$

$$\boldsymbol{\mu_K}(\boldsymbol{x}) = \boldsymbol{f}_k^T(\boldsymbol{x})\boldsymbol{\beta} + \boldsymbol{r}^T(\boldsymbol{x})\boldsymbol{R}^{-1}(\boldsymbol{y} - \boldsymbol{F}\boldsymbol{\beta}) \tag{A6}$$

$$\boldsymbol{\sigma_K^2}(\boldsymbol{x}) = \sigma^2(1 - \boldsymbol{r}^T(\boldsymbol{x})\boldsymbol{R}^{-1}\boldsymbol{r}(\boldsymbol{x}) + (\boldsymbol{F}^T\boldsymbol{R}^{-1}\boldsymbol{r}(\boldsymbol{x}) - \boldsymbol{f}_k(\boldsymbol{x}))^T(\boldsymbol{F}^T\boldsymbol{R}^{-1}\boldsymbol{F})^{-1}(\boldsymbol{F}^T\boldsymbol{R}^{-1}\boldsymbol{r}(\boldsymbol{x}) - \boldsymbol{f}_k(\boldsymbol{x}))) \tag{A7}$$

where $\boldsymbol{F}$ is the matrix of basis functions $\boldsymbol{f}_k(\boldsymbol{x})$ evaluated at known training samples, i.e. $\boldsymbol{F}_{ij} = \boldsymbol{f}_{k_j}(\boldsymbol{x}_i)$, $i = 1,2,\dots,m$; $j = 1,2,\dots,p$. $\boldsymbol{r}(\boldsymbol{x})$ is the vector of correlations between known training samples $\boldsymbol{x}_i$ and an unknown point $\boldsymbol{x}$: $\boldsymbol{r}_i = \boldsymbol{R}(\boldsymbol{x},\boldsymbol{x}_i,\boldsymbol{\theta})$, $i = 1,2 \dots m$. $\boldsymbol{R}$ is the autocorrelation matrix for known training samples: $\boldsymbol{R}_{ij} = \boldsymbol{R}(\boldsymbol{x}_i,\boldsymbol{x}_j,\boldsymbol{\theta})$, $i = 1,2,\dots,m; j = 1,2,\dots,m$. The stochastic response $\boldsymbol{K}(\boldsymbol{x})$ can then be represented using a normal distribution as,

$$\boldsymbol{K}(\boldsymbol{x}) \sim N\left(\mu_K(\boldsymbol{x}), \sigma_K^2(\boldsymbol{x})\right) \tag{A8}$$

According to this model, response predictions of samples close to known training samples will have higher confidence compared to those that are further away from the training samples. The probabilistic information provided by the Kriging model including the expected value of predictions and their variance can be leveraged to select next evaluation samples in the reliability estimation more effectively. This statistical property has been used in adaptive Kriging reliability analysis for sequential selection of training samples for model refinement.

Acknowledgments

This research has been partly funded by 'Shuimu Tsinghua Scholar' Plan through award 2020SM006 and Chinese Postdoctoral International Exchange Program through award YJ20210126 and the U.S. National Science Foundation (NSF) through awards CMMI-1635569, 1762918, and 2000156. This work was also supported in part by the Lichtenstein endowment fund at The Ohio State University. These supports are greatly appreciated.

References

[1] Z. Wang, A. Shafieezadeh, X. Xiao, X. Wang, and Q. Li, "Optimal Monitoring Location for Tracking Evolving Risks to Infrastructure Systems: Theory and Application to Tunneling Excavation Risk," *Reliab. Eng. Syst. Saf.*, p. 108781, Aug. 2022, doi: 10.1016/j.ress.2022.108781.

[2] D. Li and J. Zhang, "Stochastic finite element model updating through Bayesian approach with unscented transform," *Struct. Control Health Monit.*, vol. n/a, no. n/a, p. e2972, doi: 10.1002/stc.2972.

[3] Beck J. L. and Katafygiotis L. S., "Updating Models and Their Uncertainties. I: Bayesian Statistical Framework," *J. Eng. Mech.*, vol. 124, no. 4, pp. 455–461, Apr. 1998, doi: 10.1061/(ASCE)0733-9399(1998)124:4(455).

[4] Beck James L. and Au Siu-Kui, "Bayesian Updating of Structural Models and Reliability using Markov Chain Monte Carlo Simulation," *J. Eng. Mech.*, vol. 128, no. 4, pp. 380–391, Apr. 2002, doi: 10.1061/(ASCE)0733-9399(2002)128:4(380).

[5] D. G. Giovanis, I. Papaioannou, D. Straub, and V. Papadopoulos, "Bayesian updating with subset simulation using artificial neural networks," *Comput. Methods Appl. Mech. Eng.*, vol. 319, pp. 124–145, Jun. 2017, doi: 10.1016/j.cma.2017.02.025.

[6] Straub Daniel and Papaioannou Iason, "Bayesian Updating with Structural Reliability Methods," *J. Eng. Mech.*, vol. 141, no. 3, p. 04014134, Mar. 2015, doi: 10.1061/(ASCE)EM.1943-7889.0000839.

[7] W. Betz, I. Papaioannou, J. L. Beck, and D. Straub, "Bayesian inference with Subset Simulation: Strategies and improvements," *Comput. Methods Appl. Mech. Eng.*, vol. 331, pp. 72–93, Apr. 2018, doi: 10.1016/j.cma.2017.11.021.

[8] Ching Jianye and Chen Yi-Chu, "Transitional Markov Chain Monte Carlo Method for Bayesian Model Updating, Model Class Selection, and Model Averaging," *J. Eng. Mech.*, vol. 133, no. 7, pp. 816–832, Jul. 2007, doi: 10.1061/(ASCE)0733-9399(2007)133:7(816).

[9] Betz Wolfgang, Papaioannou Iason, and Straub Daniel, "Transitional Markov Chain Monte Carlo: Observations and Improvements," *J. Eng. Mech.*, vol. 142, no. 5, p. 04016016, May 2016, doi: 10.1061/(ASCE)EM.1943-7889.0001066.

[10] S.-K. Au and J. L. Beck, "Estimation of small failure probabilities in high dimensions by subset simulation," *Probabilistic Eng. Mech.*, vol. 16, no. 4, pp. 263–277, 2001.

[11] S. K. Au and J. L. Beck, "Subset simulation and its application to seismic risk based on dynamic analysis," *J. Eng. Mech.*, vol. 129, no. 8, pp. 901–917, 2003.

[12] Y. Zhao and Z. Wang, "Subset simulation with adaptable intermediate failure probability for robust reliability analysis: an unsupervised learning-based approach," *Struct. Multidiscip. Optim.*, vol. 65, no. 6, p. 172, Jun. 2022, doi: 10.1007/s00158-022-03260-7.

[13] Z. Wang and A. Shafieezadeh, "Metamodel-based subset simulation adaptable to target computational capacities: the case for high-dimensional and rare event reliability analysis," *Struct. Multidiscip. Optim.*, Apr. 2021, doi: 10.1007/s00158-021-02864-9.

[14] D. Straub, I. Papaioannou, and W. Betz, "Bayesian analysis of rare events," *J. Comput. Phys.*, vol. 314, pp. 538–556, Jun. 2016, doi: 10.1016/j.jcp.2016.03.018.

[15] D. J. Jerez, H. A. Jensen, and M. Beer, "An effective implementation of reliability methods for Bayesian model updating of structural dynamic models with multiple uncertain parameters," *Reliab. Eng. Syst. Saf.*, p. 108634, Jun. 2022, doi: 10.1016/j.ress.2022.108634.

[16] C. Dang, P. Wei, M. G. R. Faes, M. A. Valdebenito, and M. Beer, "Parallel adaptive Bayesian quadrature for rare event estimation," *Reliab. Eng. Syst. Saf.*, vol. 225, p. 108621, Sep. 2022, doi: 10.1016/j.ress.2022.108621.

[17] R. Schneider, S. Thöns, and D. Straub, "Reliability analysis and updating of deteriorating systems with subset simulation," *Struct. Saf.*, vol. 64, pp. 20–36, Jan. 2017, doi: 10.1016/j.strusafe.2016.09.002.

[18] S. Rahrovani, S.-K. Au, and T. Abrahamsson, "Bayesian Treatment of Spatially-Varying Parameter Estimation Problems via Canonical BUS," in *Model Validation and Uncertainty Quantification, Volume 3*, Springer, Cham, 2016, pp. 1–13. doi: 10.1007/978-3-319-29754-5_1.

[19] H. A. Jensen and D. J. Jerez, “A Bayesian model updating approach for detection-related problems in water distribution networks,” *Reliab. Eng. Syst. Saf.*, vol. 185, pp. 100–112, May 2019, doi: 10.1016/j.ress.2018.12.014.
[20] S. Shuto and T. Amemiya, “Sequential Bayesian inference for Weibull distribution parameters with initial hyperparameter optimization for system reliability estimation,” *Reliab. Eng. Syst. Saf.*, vol. 224, p. 108516, Aug. 2022, doi: 10.1016/j.ress.2022.108516.
[21] Y. Zhao, W. Gao, and C. Smidts, “Sequential Bayesian inference of transition rates in the hidden Markov model for multi-state system degradation,” *Reliab. Eng. Syst. Saf.*, vol. 214, p. 107662, Oct. 2021, doi: 10.1016/j.ress.2021.107662.
[22] K. Kim, G. Lee, K. Park, S. Park, and W. B. Lee, “Adaptive approach for estimation of pipeline corrosion defects via Bayesian inference,” *Reliab. Eng. Syst. Saf.*, vol. 216, p. 107998, Dec. 2021, doi: 10.1016/j.ress.2021.107998.
[23] Z. Pang, X. Si, C. Hu, D. Du, and H. Pei, “A Bayesian Inference for Remaining Useful Life Estimation by Fusing Accelerated Degradation Data and Condition Monitoring Data,” *Reliab. Eng. Syst. Saf.*, vol. 208, p. 107341, Apr. 2021, doi: 10.1016/j.ress.2020.107341.
[24] Z. Wang and A. Shafieezadeh, “Highly efficient Bayesian updating using metamodels: An adaptive Kriging-based approach,” *Struct. Saf.*, vol. 84, p. 101915, May 2020, doi: 10.1016/j.strusafe.2019.101915.
[25] Y. Liu, L. Li, and S. Zhao, “Efficient Bayesian updating with two-step adaptive Kriging,” *Struct. Saf.*, vol. 95, p. 102172, Mar. 2022, doi: 10.1016/j.strusafe.2021.102172.
[26] X. Xiao, Q. Li, and Z. Wang, “A novel adaptive importance sampling algorithm for Bayesian model updating,” *Struct. Saf.*, vol. 97, p. 102230, Jul. 2022, doi: 10.1016/j.strusafe.2022.102230.
[27] C. Song, Z. Wang, A. Shafieezadeh, and R. Xiao, “BUAK-AIS: Efficient Bayesian Updating with Active learning Kriging-based Adaptive Importance Sampling,” *Comput. Methods Appl. Mech. Eng.*, vol. 391, p. 114578, Mar. 2022, doi: 10.1016/j.cma.2022.114578.
[28] Y. Zhao, H. Hu, C. Song, and Z. Wang, “Predicting compressive strength of manufactured-sand concrete using conventional and metaheuristic-tuned artificial neural network,” *Measurement*, vol. 194, p. 110993, May 2022, doi: 10.1016/j.measurement.2022.110993.
[29] V. J. Romero, L. P. Swiler, and A. A. Giunta, “Construction of response surfaces based on progressive-lattice-sampling experimental designs with application to uncertainty propagation,” *Struct. Saf.*, vol. 26, no. 2, pp. 201–219, 2004.
[30] A. A. Giunta, J. M. McFarland, L. P. Swiler, and M. S. Eldred, “The promise and peril of uncertainty quantification using response surface approximations,” *Struct. Infrastruct. Eng.*, vol. 2, no. 3–4, pp. 175–189, 2006.
[31] W. Zhao, F. Fan, and W. Wang, “Non-linear partial least squares response surface method for structural reliability analysis,” *Reliab. Eng. Syst. Saf.*, vol. 161, pp. 69–77, May 2017, doi: 10.1016/j.ress.2017.01.004.
[32] G. Blatman and B. Sudret, “An adaptive algorithm to build up sparse polynomial chaos expansions for stochastic finite element analysis,” *Probabilistic Eng. Mech.*, vol. 25, no. 2, pp. 183–197, 2010.
[33] J.-M. Bourinet, “Rare-event probability estimation with adaptive support vector regression surrogates,” *Reliab. Eng. Syst. Saf.*, vol. 150, pp. 210–221, 2016.
[34] C. Song, A. Shafieezadeh, and R. Xiao, “High-Dimensional Reliability Analysis with Error-Guided Active-Learning Probabilistic Support Vector Machine: Application to Wind-Reliability Analysis of Transmission Towers,” *J. Struct. Eng.*, vol. 148, no. 5, p. 04022036, May 2022, doi: 10.1061/(ASCE)ST.1943-541X.0003332.
[35] C. Zhang and A. Shafieezadeh, “Simulation-free reliability analysis with active learning and Physics-Informed Neural Network,” *Reliab. Eng. Syst. Saf.*, vol. 226, p. 108716, Oct. 2022, doi: 10.1016/j.ress.2022.108716.
[36] B. Echard, N. Gayton, and M. Lemaire, “AK-MCS: an active learning reliability method combining Kriging and Monte Carlo simulation,” *Struct. Saf.*, vol. 33, no. 2, pp. 145–154, 2011.

[37] W. Fauriat and N. Gayton, "AK-SYS: An adaptation of the AK-MCS method for system reliability," *Reliab. Eng. Syst. Saf.*, vol. 123, pp. 137–144, 2014.

[38] I. Kaymaz, "Application of kriging method to structural reliability problems," *Struct. Saf.*, vol. 27, no. 2, pp. 133–151, 2005.

[39] B. Gaspar, A. P. Teixeira, and C. G. Soares, "Assessment of the efficiency of Kriging surrogate models for structural reliability analysis," *Probabilistic Eng. Mech.*, vol. 37, pp. 24–34, Jul. 2014, doi: 10.1016/j.probengmech.2014.03.011.

[40] Z. Wang and A. Shafieezadeh, "REAK: Reliability analysis through Error rate-based Adaptive Kriging," *Reliab. Eng. Syst. Saf.*, vol. 182, pp. 33–45, Feb. 2019, doi: 10.1016/j.ress.2018.10.004.

[41] A. Tarantola, *Inverse Problem Theory and Methods for Model Parameter Estimation*. Society for Industrial and Applied Mathematics, 2005. doi: 10.1137/1.9780898717921.

[42] M. K. Vakilzadeh, Y. Huang, J. L. Beck, and T. Abrahamsson, "Approximate Bayesian Computation by Subset Simulation using hierarchical state-space models," *Mech. Syst. Signal Process.*, vol. 84, pp. 2–20, Feb. 2017, doi: 10.1016/j.ymssp.2016.02.024.

[43] Z. Wang and A. Shafieezadeh, "Confidence Intervals for Failure Probability Estimates in Adaptive Kriging-based Reliability Analysis," *Reliab. Eng. Syst. Saf.*.

[44] J. Wang, Z. Sun, Q. Yang, and R. Li, "Two accuracy measures of the Kriging model for structural reliability analysis," *Reliab. Eng. Syst. Saf.*, vol. 167, pp. 494–505, Nov. 2017, doi: 10.1016/j.ress.2017.06.028.

[45] V. Dubourg, B. Sudret, and F. Deheeger, "Metamodel-based importance sampling for structural reliability analysis," *Probabilistic Eng. Mech.*, vol. 33, pp. 47–57, Jul. 2013, doi: 10.1016/j.probengmech.2013.02.002.

[46] M. Lázaro-Gredilla, J. Quiñonero-Candela, C. E. Rasmussen, and A. R. Figueiras-Vidal, "Sparse Spectrum Gaussian Process Regression," p. 17.

[47] S. N. Lophaven, H. B. Nielsen, and J. Søndergaard, "Aspects of the matlab toolbox DACE," Informatics and Mathematical Modelling, Technical University of Denmark, DTU, 2002. Accessed: May 14, 2017. [Online]. Available: http://orbit.dtu.dk/fedora/objects/orbit:78548/datastreams/file_2837944/content

[48] W. Betz, I. Papaioannou, and D. Straub, "Adaptive variant of the BUS approach to Bayesian updating," 06-02.07 2014.

[49] K.-V. Yuen, J. L. Beck, and L. S. Katafygiotis, "Efficient model updating and health monitoring methodology using incomplete modal data without mode matching," *Struct. Control Health Monit.*, vol. 13, no. 1, pp. 91–107, 2006, doi: 10.1002/stc.144.

[50] "UQLab sensitivity analysis user manual," *UQLab, the Framework for Uncertainty Quantification*. http://www.uqlab.com/userguide-reliability (accessed May 13, 2017).

[51] "UQLab Kriging (Gaussian process modelling) manual," *UQLab, the Framework for Uncertainty Quantification*. http://www.uqlab.com/userguidekriging (accessed May 13, 2017).

[52] V. Dubourg, B. Sudret, and J.-M. Bourinet, "Reliability-based design optimization using kriging surrogates and subset simulation," *Struct. Multidiscip. Optim.*, vol. 44, no. 5, Art. no. 5, Nov. 2011, doi: 10.1007/s00158-011-0653-8.

[53] Z. Wang and A. Shafieezadeh, "ESC: an efficient error-based stopping criterion for kriging-based reliability analysis methods," *Struct. Multidiscip. Optim.*, vol. 59, no. 5, Art. no. 5, May 2019, doi: 10.1007/s00158-018-2150-9.

[54] C. Zhang, Z. Wang, and A. Shafieezadeh, "Error Quantification and Control for Adaptive Kriging-Based Reliability Updating with Equality Information," *Reliab. Eng. Syst. Saf.*, vol. 207, p. 107323, Mar. 2021, doi: 10.1016/j.ress.2020.107323.

[55] Z. Wang and A. Shafieezadeh, "Real-time high-fidelity reliability updating with equality information using adaptive Kriging," *Reliab. Eng. Syst. Saf.*, vol. 195, p. 106735, Mar. 2020, doi: 10.1016/j.ress.2019.106735.

[56] C. Zhang, C. Song, and A. Shafieezadeh, "Adaptive reliability analysis for multi-fidelity models using a collective learning strategy," *Struct. Saf.*, vol. 94, p. 102141, Jan. 2022, doi: 10.1016/j.strusafe.2021.102141.

[57] S. N. Lophaven, H. B. Nielsen, and J. Søndergaard, "DACE-A Matlab Kriging toolbox, version 2.0," 2002. Accessed: May 13, 2017. [Online]. Available: http://orbit.dtu.dk/fedora/objects/orbit:78328/datastreams/file_2781272/content

[58] S. N. Lophaven, H. B. Nielsen, and J. Søndergaard, "Aspects of the matlab toolbox DACE," Informatics and Mathematical Modelling, Technical University of Denmark, DTU, 2002. Accessed: May 13, 2017. [Online]. Available: http://orbit.dtu.dk/fedora/objects/orbit:78548/datastreams/file_2837944/content